Synthesis, Characterizations, and Evaluation of Mechanical Properties of (Mg-Co-Ni-Cu-Zn)O High-Entropy Oxide

By

Matusal Meja Mekuria

A Thesis Submitted to

The Department of Materials Science and Engineering

School of Mechanical, Chemical and Materials Engineering

Presented in Partial Fulfillment of the Requirement for the Degree of Master's in Materials Science and Engineering

Office of Postgraduate Studies

Adama Science and Technology University

Adama, Ethiopia

December 2020 G.C

Synthesis, Characterizations and Evaluation of Mechanical Properties of (Mg-Co-Ni-Cu-Zn)O High-Entropy Oxide

By

Matusal Meja Mekuria

Advisor

Dr. Temesgen Debelo (Ph.D.)

Co-Advisor

Dr. Fikadu Gochole (Ph.D.)

A Thesis Submitted to

The Department of Materials Science and Engineering

School of Mechanical, Chemical and Materials Engineering

Presented in Partial Fulfillment of the Requirement for the Degree of Master's in Materials Science and Engineering

Office of Postgraduate Studies

Adama Science and Technology University

Adama, Ethiopia

December 2020 G.C

DECLARATION

I hereby declare that this M.Sc. thesis work entitled ***"Synthesis, Characterizations, and Evaluation of Mechanical Properties of (Mg-Co-Ni-Cu-Zn)O High-Entropy Oxide"*** is my original work and has not been presented for a degree in any other university, and all sources of material used for this thesis have been duly acknowledged.

Name of Student	Signature	Date

This M.Sc. thesis has been submitted for examination with our approval as thesis advisors.

Name of Advisor	Signature	Date
Name of Co-Advisor	Signature	Date

ADVISO RS APPROVAL SHEET

To: Materials Science and Engineering Department

Subject: Thesis Submission

This is to certify that the thesis entitled "***Synthesis, Characterizations, and Evaluation of Mechanical Properties of (Mg-Co-Ni-Cu-Zn)O High-Entropy Oxide***" submitted in partial fulfillment of the requirements for the degree of Master's in Adama Science and Technology University, the Graduate Program of the Department of Materials Science and Engineering, and has been carried out by **Matusal Meja Mekuria,** ID No: PGR/18057/11, under our supervision. Therefore, we recommend that the student has fulfilled the requirements and hence hereby he can submit the thesis to the department.

Name of Advisor	Signature	Date
Name of Co-Advisor	Signature	Date

APPROVAL OF BOARD OF EXAMINERS

We, the undersigned, members of the Board of Examiners of the final open defense by **Matusal Meja Mekuria** ID No: PGR/18057/11 have read and evaluated his thesis entitled "***Synthesis, Characterizations, and Evaluation of Mechanical Properties of (Mg-Co-Ni-Cu-Zn)O High-Entropy Oxide***" and examined the candidate. Therefore, this is to certify that the thesis has been accepted in partial fulfillment of the requirement of the Degree of Masters of Science in Materials Science and Engineering.

Advisor	Signature	Date
Internal Examiner & Chairperson	Signature	Date
Internal Examiner	Signature	Date
External Examiner	Signature	Date
Head of Department	Signature	Date
School Dean	Signature	Date
Postgraduate Dean	Signature	Date

ACKNOWLEDGMENT

First of all, the extraordinary and special thanks to the **Almighty God** for his unlimited help throughout my long journey. Next, I would like to express my deep sense of gratitude to my advisor Dr. Temesgen Debelo, for his invaluable advice, logical way of thinking, and inspiring guidance have provided a good basis for the success of this research work. Additionally, I would like to express my gratitude to my co-advisor Dr. Fikadu Gochole, for his relevant guidance and suggestions during the process of carrying out this thesis.

I would like to express my heartfelt thanks and appreciation to Dr. Dinsefa Mensur, the head of the Materials Science and Engineering (MSE) department, for his constructive criticism, valuable suggestions, and overall guidance throughout the whole studies. And my special thanks goes to Mr. Demeke Tesfaye, for his inspiring support and facilitation throughout all of the lab activities of my thesis work. I am feeling grateful and thanks to all staff members of the MSE Department; especially, Miss Biruktait Ayele, Mr. Henok Girma, and Mr. Andualem Merga, for their kindly encouragement and truly friendship supports throughout this research work.

I am really thankful to the Defense University, College of Engineering for allowing me to pursue my Master's Degree in ASTU and I also like to acknowledge their financial support. Besides this, I greatly acknowledge the facilities and working environment provided by the Department of Materials Science and Engineering in ASTU during the studies.

I found no words to express my deepest gratitude to my families, especially my mother **Kumete Guche** for her never-ending love, effort, blessing, and supporting me spiritually throughout my life; she has a lion's share in my achievements. Last but not least, I would like to acknowledge all of my friends: especially Mr. Atnafu Abrham and Mr. Yiene Molla for their kindly encouragement, motivating me, and shared their helpful thoughts for the achievement of my thesis work.

ABSTRACT

High-entropy oxides (HEOs) are among the novel family of advanced ceramic materials with attractive and unexpected functional properties in a specific area. Even though high-entropy binary oxides are very important for energy applications, the mechanical properties and thermal stability of these classes of materials are not well investigated. Therefore, in this work, HEO systems were synthesized by using a solid-state reaction method at high temperatures, from binary oxides of MgO, CoO, NiO, CuO, and ZnO, where these individual oxides were synthesized from their respective precursors through Co-precipitation methods. The binary oxides were mixed according to their stoichiometric ratio and ball-milled for 10 h; followed by filtering and drying at 100 ℃. The dried powder of the mixture was calcined sequentially at the temperature ranges from 750 to 1100 ℃, with 50 ℃ increments, to obtain optimum temperature for the resulting single-phase HEOs. To avoid phase separation, samples were quickly removed from the furnace and followed by air cooling. The phase-stability and compositional analysis of the calcined powder were performed using X-ray powder diffraction (XRD). Thus, the sample calcined at 950 ℃ can be easily indexed with a single-phase, rock-salt structure with the space group of Fm-3m. Then, the uncalcined powder was uniaxially pressed into pellets under a pressure of 45 MPa and subjected to sintering at various temperatures in the ranges from 900 to 1200 ℃ with sintering times from 3-15 h to obtain a single-phase of HEOs (Mg-Co-Ni-Cu-Zn)O. Consequently, the phase-stability of sintered pellets was confirmed using XRD, and as the result shown that pure single-phase HEOs were obtained at 1200 ℃ which are well-matched with powder calcined at 950 ℃. The microstructural and elemental analysis of the sintered pellet was characterized using Scanning Electron Microscopy (SEM) and Energy-Dispersive X-ray spectroscopy (EDX). Thermal stability analysis of the HEO powder samples was analyzed using Thermo-gravimetric analysis (TGA) and Differential thermal analysis (DTA). Finally, the mechanical properties such as compressive strength and Vickers hardness tests, which are directly correlated with the microstructure of the samples, were performed on the sintered HEO samples. The sample sintered at 1200 ℃ for 15 h showed a maximum compressive strength and Vickers hardness of about 270.09 MPa and 15.10 GPa respectively, with a corresponding relative density of about 99.20 %. Hence, these single-phase HEO materials could be a potential candidate for structural applications.

Keywords: *High-Entropy, Binary Oxides, Thermal Stability, Single-phase.*

TABLE OF CONTENTS

LIST OF TABLES

LIST OF FIGURES

LIST OF ABBREVIATIONS AND ACRONYMS

CoO	Cobalt Oxide
CuO	Copper Oxide
DSC	Differential Scanning Calorimetry
DTA	Differential Thermal Analysis
EDX	Energy-Dispersive X-Ray
HDPE	High-Density Polyethylene
HE	High-Entropy
HEA	High-Entropy Alloys
HEBM	High Energy Ball-Milling
HECs	High-Entropy Carbides
HENs	High-Entropy Nitrides
HEOs	High-Entropy Oxides
HTBF	High-Temperature Box Furnace
M-Eos	Multi-principal Equimolar Oxides
ME-REOs	Multicomponent Equiatomic Rare Earth Oxides
M-ESOs	Multicomponent Equiatomic Entropy-Stabilized Oxides
MgO	Magnesium Oxide
NiO	Nickel Oxide
SEM	Scanning Electron Microscopy
TEM	Transmission Electron Microscopy
TGA	Thermo-gravimetric Analysis
XRD	X-Ray Diffraction
ZnO	Zinc Oxide
ΔS_{config}	Configurational Entropy

1. INTRODUCTION

1.1 Background of the Study

The concept of high-entropy (HE) materials has been one of the most influential ones and gained significant interest in the field of materials science due to their unique and novel structural characteristics for a broad range of applications from structural to functional [1-3]. It provides a new point of view to develop advanced materials, which may potentially break the properties' limits of traditional materials [4, 5]. HE materials started with the development of the first high-entropy alloys (HEAs), which differ from traditional alloys. HEAs were initially defined as alloys containing multiple principal elements (five or more elements) in near to equimolar ratios by Jien-Wei Yeh in 2004 [6]. This definition has been more broadened and currently, the idea of multicomponent entropy-stabilized solid solutions was not only limited to metallic materials [7]. It was successfully applied to a new class of advanced ceramic materials, such as high-entropy carbides (HECs), nitrides (HENs), and oxides (HEOs) [8-12]. According to the literature [13], the various advantages of high-entropy ceramics are based on their compositional and structural diversity, and many of them have a wide bandgap, which makes them potential functional materials for a wide range of specific applications in the field of materials. Based on the research work of high-entropy materials [8, 14], it was recently extended to oxide ceramics, which has been observed that high configurational entropy can be effectively used to stabilize a single-phase rock-salt crystal structures containing five different cations in near to equiatomic amount.

High-entropy oxides (HEOs) are analogous to high-entropy alloys that have been established to classify entropy-stabilized solid solutions of nearly equimolar multi-component oxide systems in a single-phase, due to their high contributions of configurational entropy [15-17]. Moreover, HEOs can be defined as single-phase oxide systems containing five or more cations, such that the configurational entropy is greater than or equal to 1.5 R ($\Delta S_{config} \geq 1.5\ R$) per mole, (where R is the universal gas constant) [18]. It is one of a compositionally complex oxide system that constitutes a promising class of materials with possibly new and largely unexplored functional properties in the field of materials selection [19, 20].

The variety of compositions (multi-component approach) for a single-phase structure allows the tailoring of their physical properties and enables unprecedented materials design and implicational potential in many fields [13, 21]. Furthermore, when a sufficiently large number of (at least five) binary oxides are mixed and calcined at high temperatures; the main contribution of the total Gibbs free energy becomes governed by that of the configurational entropy [22]. Besides, it leads to the formation of a single-phase structure, with the random occupation of the cations on the specific sub-lattices, and which can be "frozen" at room temperature by rapid cooling. Due to this process, the materials having an accepted composition of HEO (Mg-Co-Ni-Cu-Zn)O, was obtained by annealing a mixture of the equivalent binary oxides at the optimum temperature (T>875 °C), which followed by uniformly distribution of the cations on sub-lattices with a single-phase [8]. Despite the random distribution of cations, HEOs are structurally ordered forming simple rock-salt crystal structures in a single-phase solid solution [8, 15, 22, 23]. Hence, high-entropy oxides are not new materials; they constitute a new pattern in the development of a new class of functional materials in the specific application area, with the configurational entropy that becomes the main parameter [15].

The concepts of configurational entropy-stabilized oxides are helpful to solve the stability problem of materials in the field of materials science and engineering. According to the equation of "$G = H - TS$" (where G, H, T, and S are Gibbs free energy, enthalpy, temperature, and entropy, respectively), the phase of a multi-component mixture with the lowest Gibbs free energy will be the stable phase [22, 24]. These phenomena, due to increasing configurational entropy or minimizing the enthalpy of mixing are both favorable for the formation of a stable single-phase, which can be obtained by using nearly equal quantities of five or more principal elements [24-26]. This is well known that configurational entropy is used as the driving force for stabilization and formation of a single-phase, on various structures for the fabrication of new materials for specific applications [23, 27, 28]. The advantages of HEOs are that they have ample structural diversity with interesting properties, which form a promising novel class of materials for a broad range of applications (from structural to functional) [13]. Besides, HEO materials have extremely high melting temperatures, hardness, thermal stability, phase stability, and high strength at elevated temperatures.

Thereby, the combination of these properties makes HEO materials potential candidates for widespread structural application areas, such as spark-plug from engine parts, furnace elements, and especially for high-temperature applications. Hence, this research work focused on synthesizing and investigating a single-phase, thermal stability, and intrinsic mechanical properties, which correlated with microstructural evolutions of (Mg-Co-Ni-Cu-Zn)O high-entropy ceramic materials synthesized through conventional solid-state reaction methods for structural applications.

1.2 Statement of the Problem

Although high-entropy binary oxides of (Mg-Co-Ni-Cu-Zn)O systems are one of the most familiar and benchmark ceramic materials in entropy-stabilized oxide systems, their mechanical properties which correlated with microstructures, thermal, and phase-stability in different conditions are not well studied; due to their complex structural diversities and synthesis methods. On the other hand, the potential capabilities of those materials were not utilized for structural applications; and, there are no other reported research works regarding this issue. Hence, these ceramic materials could be a potential candidate for structural applications. Therefore, in this work, these research gaps are expected to be modified through synthesizing HEOs of the composition ($Mg_{0.2}$ $Co_{0.2}$ $Ni_{0.2}$ $Cu_{0.2}$ $Zn_{0.2}$)O systems using conventional solid-state reaction methods. Consequently, their intrinsic mechanical properties and thermal stabilities (including the formation of single-phase high-entropy oxide solid solutions) will be investigated for structural applications.

1.3 Objective(s) of the Study

1.3.1 General Objective

In this work, HEO ceramic materials of nearly equimolar (Mg-Co-Ni-Cu-Zn)O system was synthesized and characterized, followed by studies of their intrinsic mechanical properties, thermal and phase-stability for structural applications.

1.3.2 Specific Objectives

The required specific objectives are described as follows:

- To synthesize the individual binary oxides (MgO, CoO, NiO, CuO, and ZnO) and then, entropy-stabilized oxides of equimolar (Mg-Co-Ni-Cu-Zn)O system from their corresponding precursors and binary oxides respectively,
- To characterize as-synthesized individual binary oxides using X-ray diffraction (XRD) and HEOs through XRD, Scanning electron microscopy (SEM), and Energy-dispersive X-ray spectroscopy (EDX),
- To analyze the thermal and phase-stability of as-synthesized multicomponent entropy-stabilized oxides (M-ESOs) using thermal analysis methods such as Thermo-gravimetric analysis (TGA) and Differential thermal analysis (DTA),
- To investigate the mechanical properties which correlated with microstructures, such as compressive strength and hardness value of as-synthesized pellets of HEO through compression testing and Vickers hardness testing machines respectively.

1.4 Scope of the Study

This thesis work was centered on the synthesis, characterizations, and studies of microstructural, thermal, and mechanical properties of equimolar HEOs (Mg-Co-Ni-Cu-Zn)O system with the investigation of phase and thermal stability with corresponding structural applications.

1.5 Significance of the Study

The fact that material selection is a very important point in the field of engineering; because engineers have to plan for any potential consequences those certain materials may present. Similarly providing different options of materials for specific applications was another critical issue in the field of materials science and engineering. Hence, this research has significance for improving the options of materials for structural applications and the completion of this research was directly used for the industries, to fabricate ceramic products specifically high-entropy ceramics with high thermal stability and mechanical strength to enhance the performance and durability of specific components for structural applications.

1.6 Limitation of the Study

The main limitations to conducting this research are:

- Incomplete experimental setups for synthesis and characterizations of HEO samples,
- Shortages of financial matter to apply additional characterizations of samples, such as TEM and XPS for the further investigations of HEO materials in specific applications.

1.7 Organization of the Thesis

This work is organized into five chapters. The first chapter introduces the background of the thesis; statement of the problem; objectives, scope, significance, and research limitations. The second chapter presents a literature review on high-entropy oxide systems and past research activities on high-entropy oxides. The third chapter deals with the experimental methods and conditions which include topics like materials, synthesis methods, and characterization of synthesized individual binary oxides and entropy-stabilized oxides. The fourth chapter addresses the results and discussion of the experimental work. Then, the last chapter is presented to give conclusions, recommendations, and future works, which are followed by references.

2. LITERATURE REVIEW

2.1 High-Entropy Oxides

As explained above, high-entropy oxide [1, 15, 22] is entropy-stabilized of five or more different elements (5 – 13 principal cations) with an approximate range of concentrations between 5 – 35 at.%, in near to equimolar ratios. Due to their evidence of an entropy-driven structural stabilization effect, single-phase oxide system formation will be favored. Accordingly, multicomponent HEOs were formed through a new quite revolutionary concept of entropy stabilization; which was used to stabilize a certain crystal structure that can differ from the typical structures of the constituent elements, thereby increasing the configurational entropy of the resulting compounds [29, 30]. Moreover, high-entropy oxides refer to multi-cationic solid solutions that have high configurational entropies ($\Delta S_{config} \geq 1.5\ R$ or (≥ 0.0124 kJ·mol^{-1}·K^{-1}) per mole), when all cations are present in near equiatomic ratios [15, 27]. According to other reported works [15, 31], the molar configurational entropy (S_{config}) of oxide systems can be calculated using the following formula:

$$\boldsymbol{\Delta S_{config} = -R\left[\left(\sum_{i=1}^{N} X_i \ln X_i\right)_{cation\text{-}site} + \left(\sum_{j=1}^{M} X_j \ln X_j\right)_{anion\text{-}site}\right]} \qquad \textbf{(2.1)}$$

Where, $\mathbf{x_i}$ and $\mathbf{x_j}$ represent the mole fraction of elements present in the cation and anion sites respectively, and R is the universal gas constant (R = 8.314 J/mole ·K). In the case of high-entropy oxides, the anion site contribution is expected to have only a minor effect on configurational entropy (i.e., the effect of possible oxygen vacancies is not considered); due to the presence of only one anion and the cation sublattice is the only one which is altered throughout the system. Moreover, it is anticipated that the oxygen sublattice is still only occupied by oxygen and they do not participate in the mixing of high-entropy oxide system. Hence, the configurational entropy contribution of oxygen sublattice would remain ideally zero and the entire configurational entropy of the system can be considered to be solely dependent on the cations sub-lattices [18, 32, 33]. According to reported works of literature [3, 7, 34], it is confirmed that based on its configurational entropy value, entropically-stabilized metallic oxide materials were empirically classified in to:

- ✓ High-entropy metallic oxides, if "$\Delta S_{config} \geq 1.5\ R$",
- ✓ Medium-entropy metallic oxides, if "$1.5\ R > \Delta S_{config} \geq 1\ R$",

✓ Low-entropy metallic oxides if "$\Delta S_{config} < 1\ R$".

The basic and special concept of entropy-stabilized oxide is based on the possibility to stabilize a single-phase crystal structure by increasing the configurational entropy (ΔS_{config}) of the systems [8, 14]. Thereby, it can be achieved by increasing the number of elements (principal amounts), randomly distributed on the same lattice sites, which is plotted in Figure 2.1. Furthermore, ΔS_{config} attains a maximum value when all the elements are present in near to equimolar proportions [14, 15].

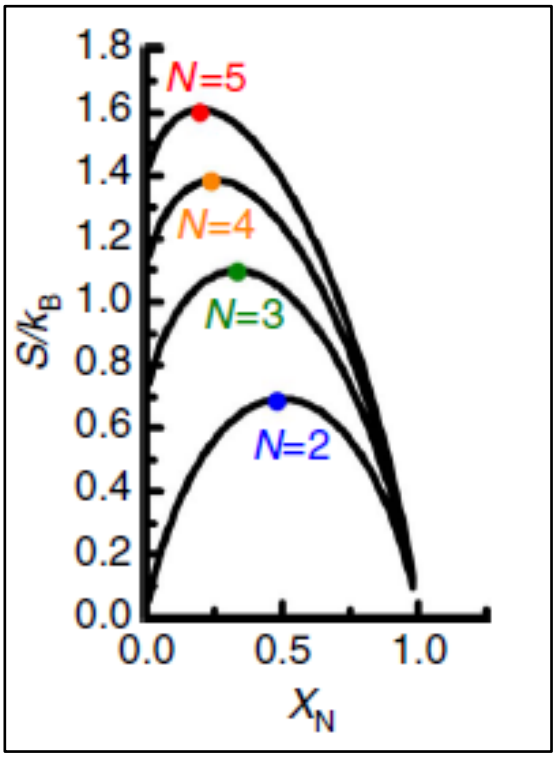

Figure 2.1: *Configurational entropy in N-component solid solutions as a function of a mole% of the Nth components [8].*

As explained above and observed that, in an equiatomic 5-cations of HEO system, the maximum configurational entropy (ΔS_{config}) value that can be achieved through the process was 1.61 *R*. Thereby, to achieve the maximum required configurational entropies of the system and to provide the appropriate diversity in structures, the 'selection rules' of cations were the most critical issues. Based on the literature [33, 35], the following 'selection criteria were considered as a guideline for the choice of cations and their compositions to provides the formation of single-phase HEO systems.

I. Similar cationic radii at a specific oxidation state and coordination number: this approach is complementary to the Hume-Rothery rules [36], for metallic systems, which was followed to minimize distortion and strain effects that can ensure complete miscibility of solid solutions in a single-phase systems,

II. All the selected metallic oxide systems should not have the same crystal structure: if all the oxides would have similar crystal structures then there would be a high probability that the multi-component system will end up in a single-phase structure same as that of the individual oxides,

III. At least one binary oxide pair should not have complete miscibility at 0.5-mole fraction based on the oxide binary phase diagram. This information was obtained from available oxide pseudo-binary phase diagrams [37, 38], and it uses the same analogy as the second criteria mentioned above, otherwise, it is quite natural for systems with complete miscibility in their binary phase diagrams to end-up as single-phase structures in multi-component combinations.

As shown in Table 2.1, the overview of crystal structures and space groups of individual oxides of the transition metal elements [33, 39] used in this study, corresponding cation oxidation state, coordination numbers, and ionic radii.[40] are presented.

Table 2.1: *Crystal structures and space groups of individual oxides, corresponding cation oxidation state, coordination numbers (CNs), and ionic radii (r_c) [40].*

Oxides	**Structure**	**Space group (number)**	**Oxidation**	**CN**	**r_c [nm]**
MgO	Rock-salt	Fm-3m (225)	2+	VI	0.72
CoO	Rock-salt	Fm-3m (225)	2+	VI	0.65[a]
NiO	Rock-salt	Fm-3m (225)	2+	VI	0.69
CuO	Tenorite	C12/c1 (15)	2+	VI	0.73
ZnO	Wurtzite	$P6_3mc$ (186)	2+	IV	0.60
ZnO[b]	Rock-salt	Fm-3m (225)	2+	VI	0.74

Where: the ***a***-indicates low spin of CoO, and ***b***-indicates the rock salt structure of ZnO is only observed at high pressures (>9 GPa) [41].

According to the selection criteria of the principal elements, both CuO and ZnO are characterized by respectively Wurtzite and Tenorite structures, which was based on the motivation to provide the appropriate diversity in structures and coordination numbers to investigate directly the entropic-stabilization in HEO systems [1, 8].

Based on the literature [42, 43], the formation of entropy-stabilized solid solution structure from a mixture of divalent MgO, CoO, NiO, CuO, and ZnO oxides confirmed the unexpected result, due to having only three of the aforementioned binary oxides can be considered as compatible, namely MgO, CoO and NiO. As shown in Table 2.1, those three binary oxides were exhibits a rock-salt structure, Fm-3m space groups with approximately similar ionic radii for all cations. But, Both CuO and ZnO are characterized by their different structures (C2/c tenorite and P63mc Wurtzite, respectively) and show limited solubility with the rest of the components. These phenomena showed that the entropic-stabilization achieved in the HEO system has a very great effect on the crystal structure. According to reported works of literature [8, 35], the material was synthesized through conventional sintering of the composing oxides followed by air cooling. The phase-stability of the synthesized system was studied at various temperatures showing an entropy-driven phase transition around a temperature of 900 ℃, which has exhibited the mentioned single-phase rock-salt structure [30, 44]. In such metals and metallic oxide systems, their high configurational entropy thermodynamically stabilizes a single-phase solid solution through a reduction of the Gibbs free energy [35, 45, 46]. Furthermore, the higher-entropy of a multi-component solid solution will lead to lower Gibbs free energy than that of a single component phase and exhibits better phase-stability at elevated temperatures [17, 26]. Based on the research works [45, 47, 48], the dependency of Gibbs free energy of mixing (ΔG_{mix}) on the enthalpy of mixing (ΔH_{mix}) and the entropy of mixing (ΔS_{mix}) in the high-entropy oxide is presented in equation 2.2.

$$\boldsymbol{\Delta G_{mix} = \Delta H_{mix} - T\Delta S_{mix}} \qquad \textbf{(2.2)}$$

In the formula, the ΔH_{mix} and $T\Delta S_{mix}$ terms can affect the free energy of the solid solution and have a completely different effect on the formation of a single-phase solid solution. ΔH_{mix} can be considered as the resistance of solid solution formation, while $T\Delta S_{mix}$ can be characterized as the driving force for single-phase solid solution, which its effect becomes stronger as the temperature increases [48-50].

Therefore, it is confirmed that a higher value of ΔS_{mix} leads to a substantial decrease of ΔG_{mix} and providing stability of the single-phases at elevated temperature [51]. As many researchers [14, 15, 31] confirmed that, a single-phase of the system was achieved if $\Delta S_{config} \geq 1.5\ R$, as then the $T\Delta S_{mix}$ can be large enough to dominate the free energy and overcome enthalpy of mixing (ΔH_{mix}). This emphasizes the fact that high temperatures are the most influential and beneficial parameters in the formation of high or medium entropy oxides of single-phase systems. Furthermore, high-entropy can reduce the Gibbs free energy and promote the formation of a single-phase solid solution, especially at high temperatures [45, 52]. Hence, under the high configurational entropy, the number of generated phases is much smaller than the maximum value determined according to the Gibbs phase law, which improves the compatibility between the components and easily forms a stable simple phase. Thereby, high-entropy can reduce the electronegativity difference, formation of some intermetallic compounds, and avoid phase separation in the solid solution. Based on the work of researchers [1, 4, 7, 31, 53, 54], the extremely fast dynamics of high-entropy alloys and metallic oxides development results from their unusual properties, which were categorized into four core effects:

I. ***Thermodynamics:*** high-entropy effects – It is one of the significant concepts of HEOs, and proposes that increased configurational entropy in near-equimolar alloys with five or more principal elements may favor single-phase solid solutions [7]. The high configurational entropy of oxide has a dominant effect on the phase of Gibb's free energy and tends to stabilize a single-phase solid solution system. Furthermore, the high-entropy effect confirmed that the higher configurational entropy can be leads to the lower free energy of a solid solution and facilitates the formation of single-phase at elevated temperatures [55]. Due to this, the mutual solubility among constituent elements was enhanced, and the number of phases present in HEOs can be reduced.

II. ***Structure:*** severe lattice distortion – atoms are randomly distributed in the crystal lattice, leading to its distortion and affecting mechanical, transport, and thermal properties. For instance, the lattice distortion effects in HEAs cause high solid solution hardening, thermal resistance, electrical resistance, and X-ray diffuse scattering [56]. In general, the lattices of high-entropy alloys (HEAs) are becoming aware to be severely distorted systems due to the presence of atoms of different sizes [7, 57].

However, severe lattice distortion is also considered to be one of the reasons for slower diffusion kinetics and high strength in HEAs [51], which effectively inhibit particle aggregations and retard crack propagation in the HEO ceramic materials.

III. ***Kinetics:*** sluggish diffusion – kinetics of cationic diffusion in high-entropy oxide is slower than that of either conventional alloys or pure metals; due to their interaction between different cations and the lattice distortions. The phase transition usually requires a synergistic diffusion rate between the components to achieve the phase separation in an equilibrium system. However, sluggish diffusion can hinder the agglomeration of the secondary particles and atomic movement, which will seriously limit the effective diffusion rate of cations in the sublattice [58, 59]. Besides, it affects the formation of new (secondary) phases in HEOs and provides the cooperative diffusion of cations to attain the uniformly distributed single-phase [60].

IV. ***Properties:*** cocktail effect – synergistic effect of properties resulting from mutual interactions among composing elements of HEO systems. Moreover, the cocktail effect has been widely demonstrated and indicating that new properties could be obtained by a complex mixture of principal elements that could not be obtained from any of these components independently.

As literature [53] stated that, all of the aforementioned factors originate from the most basic thermodynamic and structural properties of high-entropy materials. They provide high-entropy materials with numerous versatile properties and therefore make them suitable for several applications in materials engineering. In HEO ceramic materials, the entropic contributions to the free energy were higher than that of the cohesive energy, and which leads to promoting the thermodynamic stability at an optimum temperature [45]. Besides, these fundamental thermodynamic studies lead to hypothesize that, the sufficient temperature would promote an additional transition to a structure containing only one sublattice with random cation occupancy [8]. Furthermore, the existance of entropy-driven structural a single-phase solid solution of HEO (Mg-Co-Ni-Cu-Zn) O was dependent on the variations of temperatures and compositions of the systems, which are briefly investigated in Figure 2.2 and 2.3. As shown in Figure 2.2 and based on different cases, the HEO materials like (Mg-Co-Ni-Cu-Zn)O system undergoes a reversible phase transformation from single-phase solid solution to multi-phase mixture; and demixing of the rock-salt structure of the system is observed when the system is calcined at relatively

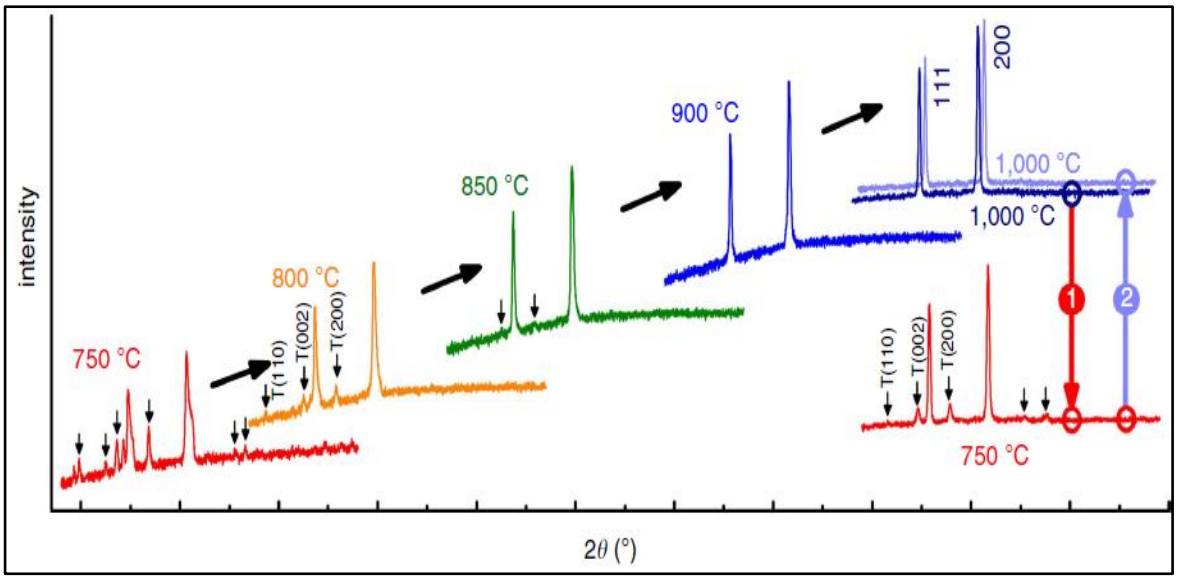

Figure 2.2: *XRD patterns for HEO systems in an equimolar mixture of binary oxides (MgO, CoO, NiO, CuO, and ZnO), with different calcination temperatures, the arrows indicate that the peaks associated with non-rocksalt phases, and (T) identify the peaks indexed with tenorite phase [8].*

lower temperatures. Secondly, the formation of single-phase structures can depend on the number of constituent cations and configurational entropy of the systems. The removal of any component oxide from the parent HEO systems, which provides a high probability for the formation of multi-phases (as shown in Figure 2.3). Besides, any deviation from equimolarity reduces the number of possible configurational entropy and also influences the phase-stability (single-phase formation) of the systems at the required temperatures.

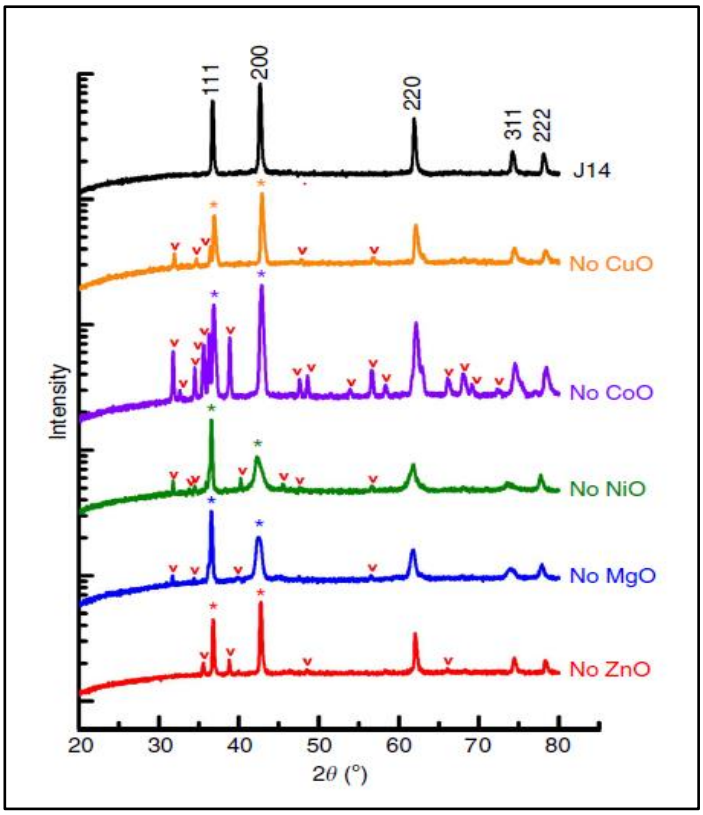

Figure 2.3: *XRD analysis of composition series where individual components are removed from the parent compositions, Asterisks indicate the peaks associated with rock salt structure while carrots identify peaks from other crystal structures [8].*

2.2 Thermal Stability of High-Entropy Oxides

Thermal stability of high-entropy oxide materials represents the ability to resist or to maintain their chemical composition and phase of the system at elevated temperatures; which are determined by using thermal analysis. Thermal analysis is a group of techniques that study the properties of materials as they change with temperature. Besides, it provides significant and relevant information for HEO systems in various conditions of the application area. Thereby, the thermal stability, weight loss, specific heat, and other material properties were determined by utilizing different characterization techniques, such as Thermo-gravimetric analysis (TGA), Differential thermal analysis (DTA), and Differential scanning Calorimetry (DSC).

TGA is an outstanding technique for characterizing the thermal properties of materials such as mineral compounds, advanced ceramics, plastics, as well as chemical and pharmaceutical products in the specific application area.

It is a technique frequently used in thermal analysis, characterizes the materials by measuring their change in mass as a function of temperature, using the range of (10 mg to 1 g) sample size, from ambient to 1000 ℃ temperature, and 0.01 to 100 ℃/minute heating rate. According to the above processes, the weight loss of samples occurs due to the changing of chemical or physical properties and can be detected down to fractions of a micro-gram. The major advantages of the methods are the simplicity of the apparatus, high sensitivity for the detection of low decomposition rates, speed of the temperature adjustment, and small sample requirement. Based on the type of sample and information required, the characterization can be performed by fixing the temperature over a range of time or by changing the temperature over a fixed time. Both of these methodologies provide information on the thermal stability of samples. The thermal properties and behavior of samples, which can be characterized by TGA including thermal stability, composition, material purity, absorbed moisture content, phase-stability, decomposition reactions, and temperatures.

In this work, thermal analyses were used to determine mainly thermal stability, decomposition reactions, phase-stability, and oxidative stability of entropy-stabilized oxide systems. Due to the formation of entropy-stabilized single-phase at elevated (optimum) temperature, high-entropy oxide materials are sufficiently thermal stable.

As recently stated in [61], entropy-stabilized metal oxides can be achieved independent of the synthesis method, at high temperatures (900-1300 ℃), and taking long times for reaction (e.g., >48 h) have typically been used to crystallize high-entropy oxide materials. Thus, the natural focus in this field has been to look for materials in which configurational disorder on a metal oxide site produces high stability at elevated temperatures. The researcher [62], has proved that the solid solution of equimolar MgO, CoO, NiO, CuO, and ZnO system of HEO calcined at the temperature of above 875 ℃ is more thermal stable than that of separated individual oxides. Next to calcination temperature, the cooling rate was the critical parameter for the formation of single-phase, i.e. the slow cooling or annealing at a temperature below 875 ℃ causes phase separation. However, if the cooling rate is high enough (rapid cooling), the metastable a single-phase rock-salt structure can be stabilized down to room temperatures.

According to [63], the entropy-stabilized single-phase oxide of (Mg-Co-Ni-Cu-Zn) O_x which is supported by Pt, can act as active sites for enhanced catalytic performance in CO oxidation through the favored dispersion. Besides, it provides exceptional thermal stability of materials operating around 900 ℃, owing to the entropy-stabilized behavior inside the metal oxides. Hence, those materials are capable of effective service in harsh conditions. The entropically-driven phase-stability of the (Pt-Mg-Co-Ni-Cu-Zn) Ox (0.3 wt% Pt) endowed the catalyst with superior activity for CO oxidation at high temperatures.

2.3 Mechanical Strength of High-Entropy Oxides

High-entropy materials were often exhibiting higher performance than that of a lower-entropy system in various aspects; such as thermal stability, fracture toughness, and high moduli of elasticity. While there are extensive research activities in the field of high-entropy alloys, comparably a few parts of it are performed for advanced ceramic materials [48]. High-entropy ceramics are a family of advanced ceramic materials such as carbide, nitride, and oxides that display a unique set of properties, including extremely high melting temperatures, high hardness, good chemical stability, and high strength at elevated temperatures [64]. But, due to the lack of ductility and their brittle nature, they have low tensile strength.

In particularly, entropy-stabilized oxide of the ceramic system is one class of the advanced ceramic materials and would have a superior combination of excellent properties; such as high strength at elevated temperatures, low density, exceptional wear, and corrosion resistance with excellent physical properties (optical, electrical and magnetic). Hence, the combination of properties makes these materials potential candidates for widespread structural application areas, such as engine manufacturing, industrial process engineering, furnace elements, hypersonic vehicles, and especially at high-temperature applications. The performance of these materials is closely related to their microstructures and synthesis conditions. Especially sintering temperatures and times were an important factor in the fabrication process of ceramic bodies; which can significantly affect their mechanical properties [65].

Many ceramics undergo a significant increase in density during sintering, which is crucial for developing desirable properties such as mechanical strength and dielectric constant [66].

Specifically, for the improvement of mechanical properties, the parameters which can be controlled by the sintering process are: density, porosity, grain size, and their distribution. Sintering is one of the most important processes for the production of compacted powders and the densification mechanism of ceramic materials [67, 68].

In the study of the strength of ceramic materials, their compressive strength is the capacity of a material or structure to offer strong resistance loads tending to reduce sizes. It can be measured by plotting applied force versus the deformation of specimen [69]. Some material fractures at their compressive strength limit while others deform irreversibly, so a given amount of deformation may be considered as the limit for compressive load [70].

The hardness values of ceramic materials are usually measured by conventional microhardness with Vickers diamond indenter. The Vickers hardness testing procedure, usually with low-load test forces, is probably the most preferable hardness testing technique for ceramics. For research purpose, Vickers and Knoop's indenters are more customary and approximately 60% of the worldwide published ceramic materials hardness values are measured through Vickers, with a typical load of 9.8 N (1 kgf) and for some soft or high toughness ceramics 98 N (10 kgf) [71]. Throughout the testing process, the machine makes impressions whose diagonal sizes were measured with attached optical microscopy. Then, the Vickers hardness (HV) value was obtained from the quotient of the applied test force and the surface area of the residual indent on the specimen. To calculate the surface area of the residual pyramidal indentation, the average of the two diagonals (d1 and d2 in mm) are used and the testing procedure is as plotted in Figure 2.4. The surface area of the indentation (A in mm^2) can be determined by using equation 2.3.

$$\boldsymbol{A = D^2/2Sin\,(136°/2)} \qquad \textbf{(2 .3)}$$

Where: D is the average length of the diagonals (d1 and d2 in mm). Then, the Vickers hardness value (HV) of the specimen is calculated by using the equation 2.4.

$$\boldsymbol{HV = F/A = 1.8544F/D^2} \qquad \textbf{(2.4)}$$

Where F is the applied loads in kilograms-force (kgf) and D is in mm, the corresponding units of HV are then kilograms-force per square millimeter (kgf/mm^2).

To calculate Vickers hardness number using SI units (in MPa) we must convert the force applied from kilogram-force (kgf) to Newton's (N) by multiplying by 9.80665 (standard gravity).

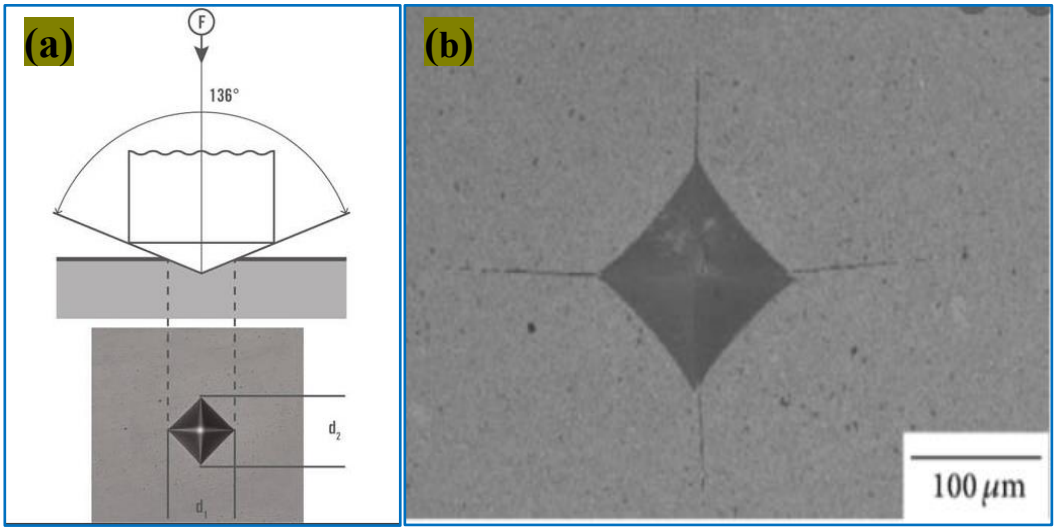

Figure 2.4: *Schematic of* ***(a)*** *the Vickers hardness testing procedure and* ***(b)*** *Optical images of Vickers indentation [71].*

Hardness is an important parameter correlating with the wear resistance of the materials. Hence, in specific applications where the wear has to be restricted, high-hardness materials such as high-entropy oxides are typically used.

2.4 Previous Works Related to High-Entropy Oxides

As explained above and observed from many works of literature, the multicomponent HEO systems provide a new quite revolutionary concept of entropy stabilized oxides through different synthesis methods for a wide range of applications. As many researchers [72-76] agreed that, there are different approaches for synthesis methods that have been developed to prepare high entropy oxides. These methods are nebulized spray pyrolysis (NSP), flame spray pyrolysis (FSP), co-precipitation (CP), hydrothermal (HT), and solution combustion synthesis (SCS) which are used to produce homogenous nanocrystalline oxides. Despite the advantages of these methods, some of them may encounter disadvantages such as the requirement of complicated equipment, complex procedures, long time reaction, high-energy consumption, and also need the handle of large amounts of organic salt, a solvent of surfactant, causing environmental pollution.

In this context, the modified solution combustion synthesis (SCS), co-precipitation (CP), and solid-state reaction methods were the most widely used approach for the synthesis of high-surface nanomaterials, such as oxides with homogenously distributed cations in sublattice [77-79]. Besides, the high-entropy oxides synthesized through the conventional solid-state reaction methods were more preferable for the synthesis of the bulk form of products with relatively cost-effective processes [75, 80]. In this method, the ball milling process was applied to mix the raw powders and to achieve the chemical and microstructural homogeneity of the oxide systems.

Based on the literature [72, 73], it has been shown that the configurational entropic contribution to the Gibbs free energy can be used for stabilizing simple crystal structure, which should normally not form solid solutions. Accordingly, HEOs of (Mg-Co-Ni-Cu-Zn)O synthesized from a mixture of equimolar five binary oxides (MgO, CoO, NiO, CuO, and ZnO) through solid-state reaction methods, with randomly distribution of the cations in a face-centered cubic lattice. Besides, at high temperatures, these mixtures of oxides form a solid solution with an unexpected rock-salt structure which is followed by rapid cooling to achieve metastable at room temperatures.

According to [72], the HEOs of (Mg-Co-Ni-Cu-Zn)O a rock-salt structure with the random occupation of the cation sites was exhibit promising dielectric properties for applications of large-k dielectric materials. As the recently reported work of literature [73, 75], the high-entropy oxide system of (Mg-Co- Ni-Cu-Zn)O doping with alkali cations, i.e., Li+ and Na+, $(Mg, Co, Ni, Cu, Zn)_{1-x}Li_xO$, $(Mg, Co, Ni, Cu, Zn)_{1-x}Na_xO$, can be synthesized by the solid-state reaction method. Due to their superionic Li+ and fast-ionic Na+ in the system, they can lead to excellent superionic conductivity. Based on this report, the high-entropy oxides mixed with monovalent cations are a very promising potentially candidate electrolyte material in solid-state batteries.

The entropy-stabilized system of (Mg-Co-Ni-Cu-Zn)O which was synthesized through solid-state reaction methods was investigated as an anode material for lithium-ion batteries, due to providing a high initial discharge specific capacity and exhibiting superior cycling stability [81]. Similarly, the HEOs of (Mg-Co-Ni-Cu-Zn)O were synthesized by nebulized spray pyrolysis methods, which have been exploited as promising negative electrode (anode) materials for Li-ion batteries, due to their robust Li-ion storage properties and cycling performance [23].

The entropy-stabilized oxides of (Mg-Co-Ni-Cu-Zn)O were synthesized through co-precipitation methods and almost fully dense ceramic obtained by sintering at relatively low temperature (1050 ℃) with a single-phase rock-salt structure [62]. Based on the reported work of literature [35, 82], the concepts of high-entropy oxides were further broadened by the discovery of multicomponent equiatomic rare-earth metallic oxides (ME-REOs), which could be successfully incorporated into a single-phase pure fluorite type crystal lattice. It has been recently shown that entropy-stabilized oxides can be extended to complex systems like multi-cations perovskite (ABO_3) with single-phases [14, 83].

3. MATERIALS, METHODS, AND CHARACTERIZATIONS

3.1 Materials

In this research work, raw materials of different chemicals, which were utilized for the synthesis of individual metallic oxides are: Magnesium Nitrate Hexahydrate (Mg $(NO_3)_2.6H_2O$) (Loba Chem, 99%,), Cobalt Nitrate Hexahydrate (Co $(NO_3)_2.6H_2O$) (Sigma Aldrich, 99%), Nickel Nitrate Hexahydrate (Ni $(NO_3)_2.6H_2O$) (Loba Chem, 99%,), Copper Sulfate Pentahydrate ($CuSO_4.5H_2O$) (Loba Chem, 99%,), and Zinc Nitrate Hexahydrate (Zn $(NO_3)_2.6H_2O$) (Sigma Aldrich, 99%). The corresponding high-entropy oxide was synthesized from Magnesium Oxide (MgO), Cobalt Oxide (CoO), Nickel Oxide (NiO), Copper Oxide (CuO), and Zinc Oxide (ZnO). Sodium Hydroxide (NaOH) and Potassium Carbonate (K_2CO_3) are used as precipitating/mineralizer agents. Moreover, precipitating agents based on hydroxides and carbonates typically produce a weakly agglomerated powder that exhibits better sintering [84, 85]. Additionally distilled water and ethanol are used for all syntheses and treatment processes (as a solvent for dissolving chemicals and for washing purposes in centrifuging processes). All chemicals (precursors) and precipitating agents were commercially purchased with analytical purity ≥ 99% which are used to prepare a high-entropy oxide system and the cations were selected according to selection criterion [33].

3.2 Synthesis Methods for Individual Metallic Oxides

In the present work, firstly individual metallic oxides (MgO, CoO, NiO, CuO, and ZnO) were synthesized by a processing route based on wet chemical synthesis methods (simple co-precipitation) from their respective precursors [62]. Because of co-precipitation method is the most common, rapid, and easier to produce individual metallic oxides. Moreover, it has a greater potential in the production of homogeneous single-phase multicomponent systems as their pH values are maintained constant throughout the process, and all the cations can be precipitated properly into a mixed hydroxide [33, 80]. The whole synthesis processes carried out by using a magnetic stirrer to form a homogeneous solution, a pH meter to adjust a solutions pH value, a centrifuging machine to wash and remove unwanted ions (impurities), a forced convectional drying oven to remove moistures (water) and muffle or high-temperature furnaces for calcination processes.

Moreover, the flow charts of synthesis procedures for individual metallic oxide particles through co-precipitation methods are summarized in Figure 3.1.

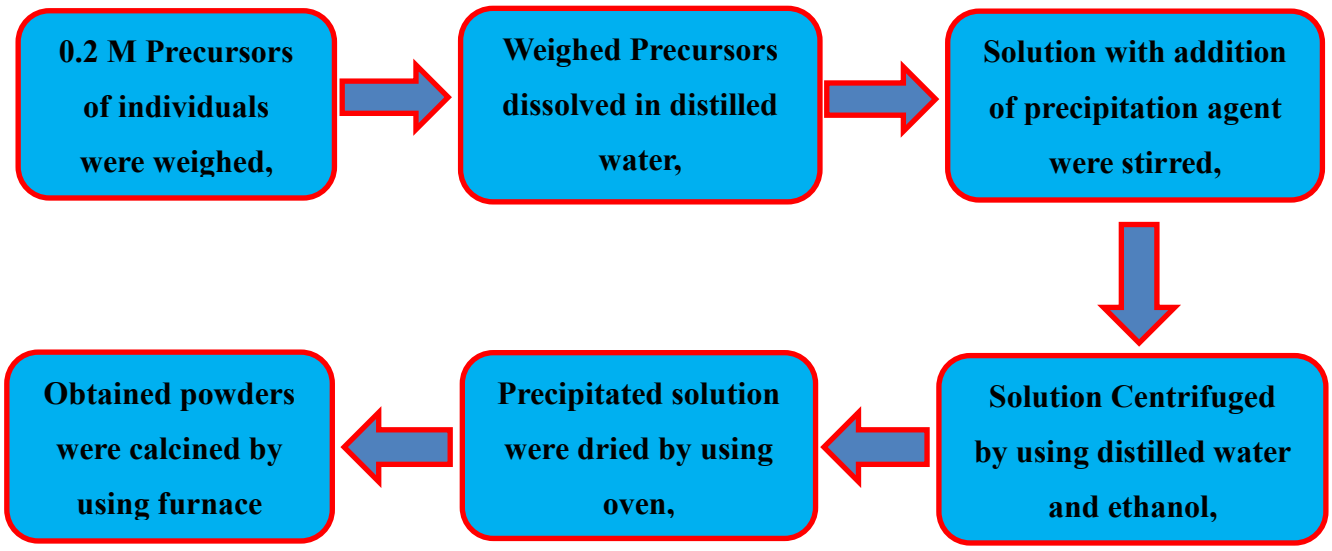

Figure 3.1: *Flow chart of synthesis procedures of individual metallic oxides.*

3.2.1 Synthesis of Magnesium Oxides (MgO)

Magnesium oxides (MgO) were synthesized using magnesium nitrate hexahydrate ($Mg(NO_3)_2.6H_2O$) as a source of Mg^{2+} ions and a precipitating agent of sodium hydroxide (NaOH) as OH^- ions source through by co-precipitation methods [86, 87]. In a typical reaction process for the growth of MgO, 0.2M of magnesium nitrate solution was prepared by using 100 ml of distilled water as a solvent and stirred at room temperature for 45 minutes using a magnetic stirrer to form a homogeneous solution. Then, 2M of NaOH dissolved in 50 ml distilled water and added dropwise into the prepared magnesium nitrate solution with continuous stirring until the pH value reached 9. The white precipitate of magnesium hydroxide appeared in the beaker after a few minutes and the stirring was continued for 60 minutes. The obtained precipitate was centrifuged and washed with distilled water and ethanol to remove the residuals, followed by drying in an oven at 100 ℃ for 3 h. Finally, the obtained powder was calcined at 600 ℃ for 4 h in a muffle furnace to get the desired MgO powders.

3.2.2 Synthesis of Cobalt Oxides (CoO)

To obtain cobalt oxides in binary oxidation state [88], initially, 0.2 M (5.821 g) of cobalt nitrate hexahydrate dissolved in 100 ml distilled water by stirring for 45 minutes at room temperature. A meanwhile, 2 M of NaOH dissolved in 100 ml distilled water and added to the solution of cobalt nitrate drop-wise under vigorous stirring until the pH value of solution reached 9. When the pH value of the solution was achieved, the pink precipitate has appeared. Then, the solution was heated at 60 ℃ and kept under constant stirring for 2 h [89]. A dark brown colored precipitate was formed at the bottom of the beaker. The obtained precipitate was filtered and washed several times by using distilled water and ethanol to get the final products. The resultant product was dried in the oven at 100 ℃ for 5 h. Finally, the obtained powder was calcined at 1000 ℃ with a rate of 10 ℃/minute for 3 h using a high-temperature box furnace; to obtain a binary oxidation state of cobalt oxide (CoO) powders. Consequently, the calcined sample was rapid cooled from 1000 ℃ to room temperature by quickly extracted from the furnace; to avoid the formation of cobalt oxides in the Co_3O_4 oxidation state [90, 91].

3.2.3 Synthesis of Nickel Oxides (NiO)

Nickel oxide nanoparticles were synthesized [92, 93], using nickel nitrate hexahydrate and sodium hydroxide as raw materials (precursors). For the typical experimental procedure, 0.2 M of $Ni(NO_3)_2.6H_2O$ was dissolved in 100 ml of distilled water under constant stirring for 1 h. Meanwhile, 2 M (4 g) of NaOH dissolved in 50 ml distilled water and added to the above solution drop by drop with continuous stirring until the pH value of the solution reached 10. This solution was stirred constantly at a temperature of 80±5 ℃ for 4 h. After completion of the reaction, the green-colored precipitate was obtained and it was thoroughly washed with distilled water and ethanol to remove all the other ions and impurities. The precipitate was dried at 80 ℃ for 12 h and crushed into a fine powder using agate mortar. Finally, the powder obtained from the above method was calcined at 600 ℃ for 4 h using a muffle furnace.

3.2.4 Synthesis of Copper Oxides (CuO)

The CuO nanoparticles were synthesized through simple co-precipitation methods [94], using copper sulfate and sodium hydroxide as precursors.

Firstly, 0.2 M (4.994 g) of $CuSO_4.5H_2O$ was dissolved in 100 ml of distilled water under constant stirring for 30 minutes. Then, 2M (4g) of NaOH was dissolved in 50 ml of distilled water and added drop by drop into $CuSO_4.5H_2O$ solution by touching the walls of the vessel under vigorous stirring until the pH value of solutions reached 12. The gradually black colored precipitate has appeared and the reaction was allowed to proceed for 2 h under constant stirring at 32 ℃ [95]. Then the solution was allowed to settle overnight and supernatant solutions were discarded carefully. The obtained precipitate was centrifuged and washed several times with distilled water and ethanol. Finally, the washed precipitate was dried at 80 ℃ for 12 h and calcined at 500 ℃ for 4 h using a muffle furnace.

3.2.5 Synthesis of Zinc Oxides (ZnO)

Zinc oxide nanoparticles were synthesized through wet chemical synthesis methods (co-precipitation) using $Zn(NO_3)_2.6H_2O$ and NaOH as starting materials [96, 97]. Firstly, 5.948 g of $Zn(NO_3)_2.6H_2O$ dissolved properly in 100 ml distilled water and stirred under an electromagnetic stirrer for 45 minutes. Then, 3M (6 g) of NaOH was prepared in 50 ml distilled water. When the temperature of $Zn(NO_3)_2.6H_2O$ solution reached 70 ℃, an aqueous solution of NaOH was added to the above solution slowly drop by drop until the pH values reached 10, and then continues stirring for 2 h. After completion of the reaction, a milky white precipitate was obtained, which is allowed to settle overnight to complete the precipitation. The resulting white precipitate was separated by centrifuge and washed several times with distilled water and ethanol. The filtered precipitate was dried at 80 ℃ for 8 h and finally, calcined at 500 ℃ for 2 h in a muffle furnace.

3.3 Synthesis Methods for High-Entropy Oxide (HEO)

High-entropy oxide samples were synthesized from individual as-synthesized binary oxides; such as MgO, CoO, NiO, CuO, and ZnO using a method of conventional solid-state reaction at high temperatures. Based on the literature [98], the starting individual binary oxide powder in stoichiometric amount (according to equation 3.1) with specific equimolar amounts of the metallic oxides were calculated and weighed by using an analytical precision balance; in order to obtain the required weight of samples for each batch. Accordingly, the total mass of the sample approximately 7.018 g was prepared for the first batch (listed in Table 3.1, and shown in Figure 3.2).

$$\boldsymbol{Mass = (n)(M_{wt})} \qquad \textbf{(3.1)}$$

Where: n = numbers of mole, M_{wt} = molecular weight of binary oxides.

The composition, molar amount, and measured mass of equimolar multicomponent high-entropy oxide samples were shown below in Table 3.1.

Table 3.1: *Measured amounts of each oxide component in the multi-components entropy-stabilized oxide system.*

Individual Binary Oxide	**Molar Amount of each Component (mol)**	**Measured Mass of each Component (g)**
MgO	0.02	0.806
CoO	0.02	1.499
NiO	0.02	1.494
CuO	0.02	1.591
ZnO	0.02	1.628
Total mass		**7.018**

The weighed HEO pre-alloyed powder was mixed by a mechanically wet form of ball milling (BM) at 320 rpm for 10 h with high-density polyethylene (HDPE) cylindrical jar; using 2 mm, and 5 mm diameters of zirconia balls as milling media in ethanol with intermittent mixing to promote reaction homogeneity [81]. To ensure adequate mixing and for attaining uniform dispersions of the constituent oxides among each other, all batches of HEO pre-alloyed powder were milled for 10 h and more.

After ball milling, the mixture was filtered and dried at a temperature of 100 ℃ for 5 h in a forced convection drying oven to remove the solvent and moisture content. The dried powder was air-cooled to room temperature and hand-milled using an Alumina Mortar with a pestle of manual smash, to obtain fine particle sizes of the pre-alloyed HEO system. Then, in the first part of the processes, the dried fine powder of the mixture was calcined sequentially at the temperatures of 750 ℃, 800 ℃, 850 ℃, 900 ℃, 950 ℃, 1000 ℃, 1050 ℃, and 1100 ℃, using high-temperature box furnace with the rate of 10 ℃/minutes for 3 h, to obtain optimum temperature for the resulting high-entropy oxides. To avoid phase separation of the mixture, all batches of samples were quickly removed from the furnace and followed by air cooling to room temperatures.

The obtained structural phase of the calcined powder was determined using an X-ray diffractometer, according to Bragg- Brentano geometry using Cu-Kα radiation, (Cu-K_{α} radiation λ = 1.5406 Å, generated at 40 kV and 30 mA). Finally, as-synthesized fine powder samples were labeled as multicomponent entropy-stabilized oxide (M-ESOs) systems, due to exhibiting a single-phase structure [99, 100].

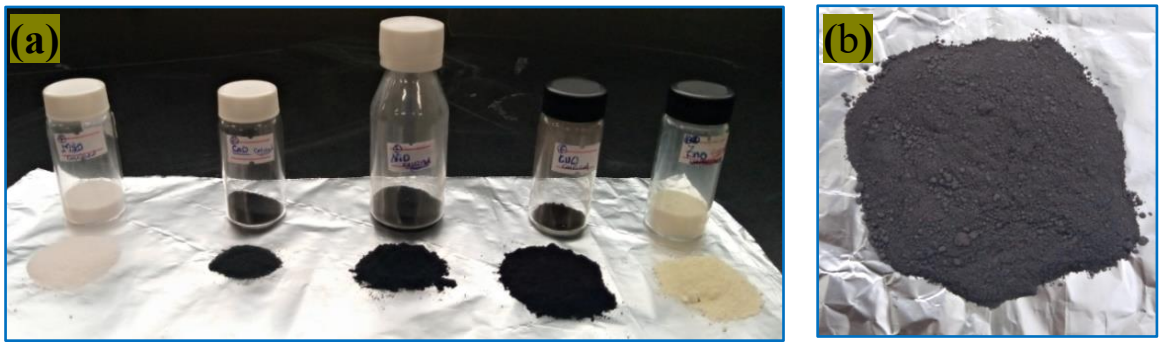

Figure 3.2: (a) *Digital camera Photographs of as-synthesized individual binary oxides powders (MgO, CoO, NiO, CuO, and ZnO respectively from left to right) showing the different colors of oxides before ball milling* ***(b)*** *Mixture of multicomponent equimolar oxides after ball-milled.*

In the second part of the processes, the well-mixed uncalcined fine powders were separated into several samples with 3.50 g per sample and then pressed into pellets with a 20 mm diameter circular press mold, using a uniaxial hydraulic Mounting press under a pressure of 45 MPa with 30 minutes compaction times. Then, the obtained HEO pre-alloyed pellets were subjected to conventional sintering at the temperatures of 900 ℃, 1000 ℃, 1100 ℃, and 1200 ℃, as labeled S_1, S_2, S_3, and S_4 respectively. These disks were sintered using in a high-temperature box furnace with a rate of 10 ℃/minute for 3 h. The sintered pellet samples were air-cooled to room temperature by direct extracted from the furnace, to avoid phase separation of the mixture of (Mg-Co-Ni-Cu-Zn)O HEOs. The digital photographs of mixed-HEO powder and prepared pellets were shown below in Figure 3.3.

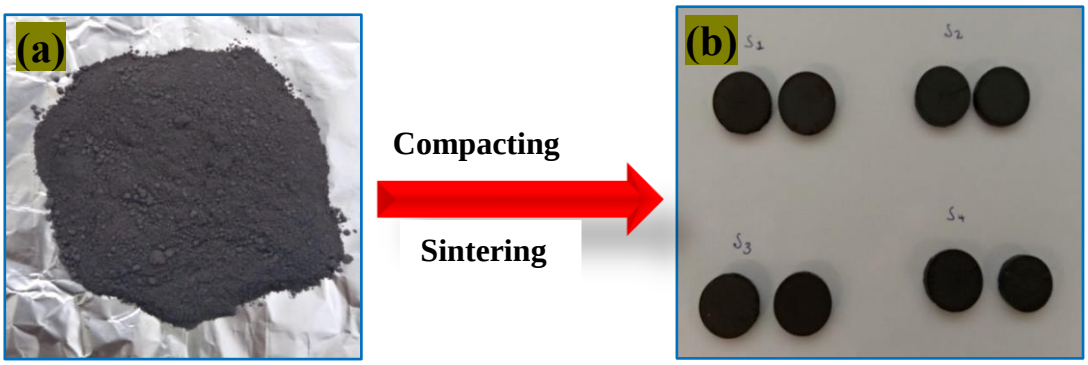

Figure 3.3: *Photographs of* ***(a)*** *as-synthesized powder of multicomponent equimolar oxides after ball milled* ***(b)*** *high temperature sintered pellets of the HEO system.*

Similarly, the second batch of pellet samples was prepared through variation of sintering temperatures and times (1100 ℃, 1200 ℃) and (9 h, 15 h) respectively; to investigate the effects of sintering temperatures with times. Moreover, the whole synthesis procedures for the individual binary oxide and HEOs through co-precipitation and solid-state reaction methods respectively were summarized below in Figure 3.4.

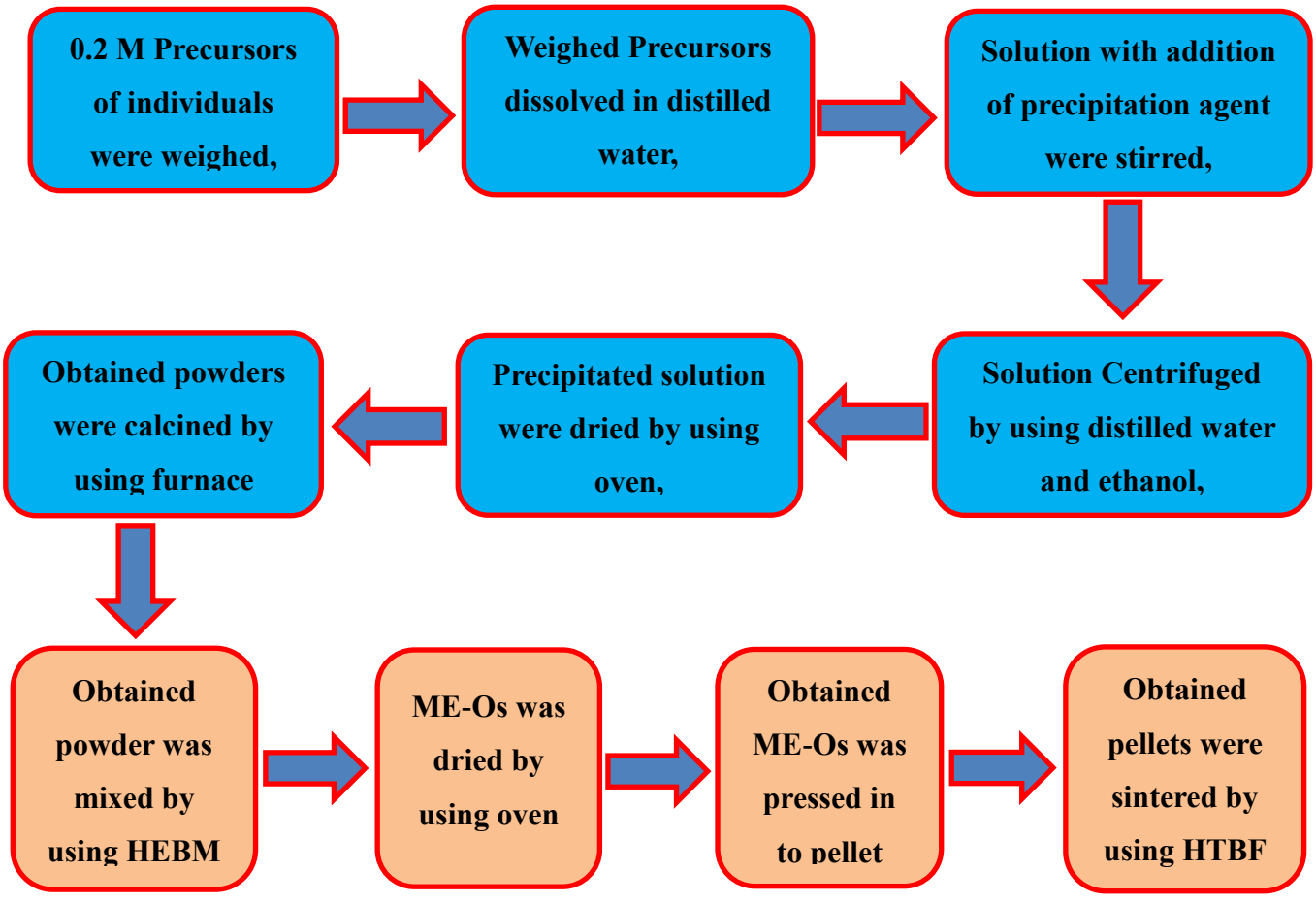

Figure 3.4: *Flow chart of synthesis procedures of individual metallic oxides and HEOs.*

The synthesized pellets were grinded, polished, and characterized by SEM to make an analysis of morphology, microstructural evolution, and porosity which correlates with the mechanical strength of HEO systems. Consequently, as-prepared pellets were milled again into fine particles by using Alumina Mortar with a pestle of manual smash. Then the obtained powder was dried in a vacuum oven and characterized X-ray diffractometer to determine the structural phase-stability of as-synthesized HEO pellets.

3.4 Characterizations

3.4.1 X-Ray Diffraction (XRD)

Synthesis and characterizations of individual binary oxides (MgO, CoO, NiO, CuO, and ZnO) were very critical and initial points for the synthesis of the equimolar high-entropy oxide system. The synthesized individual metallic oxide powder samples were characterized by X-ray diffraction to determine the crystal structure, phase-stability (purity), average crystallite size, and lattice parameters. Similarly, as-synthesized HEO powders and pressed pellets were characterized and confirmed by XRD to investigate the formation of a single-phase at the optimum temperature. Room-temperature X-ray diffraction patterns of each sample were recorded by using a diffraction instrument (XRD-7000S Shimadzu) with Cu Kα radiation, (Cu-K_{α} radiation λ = 1.5406 Å) using the operating voltage of 40 kV, a current of 30 mA, over the diffraction angle (2θ) range between 10° and 80°. Rietveld analysis (TOPAS 5, Bruker) [101] of the XRD patterns was used to determine the structure and phase composition of the as-synthesized and thermally treated powders.

3.4.2 Scanning Electron Microscopy (SEM)

The overall microstructure and elemental composition of as-synthesized entropy-stabilized oxides (Mg-Co-Ni-Cu-Zn)O powder samples, as well as the compacted pellets, were characterized using a Scanning electron microscope (SEM) and energy-dispersive X-ray spectroscopy (EDX) (Oxford Instruments X-MaxN 50 mm^2 Silicon Drift Detector) (COXIEM-30) with the operating voltage of 20 keV. Several EDX spectra were obtained and analyzed using AZtecOne software to provide better statistical results.

3.4.3 Thermal Analysis

The thermal behavior of entropy-stabilized oxide powders was analyzed by simultaneous differential thermal analysis and Thermo-gravimetric analysis (TG-DTA) measurement was performed using a thermal analysis technique (DTG-6OH Shimadzu) both in air and in an argon atmosphere at a scanning rate of 10 ℃/minute from room temperature to 1000 ℃, using α-Al_2O_3 as reference. Thermo-gravimetric analysis (TGA) was used to monitor the weight loss of the samples as a function of temperature or time to investigate the thermal stability of HEO.

3.4.4 Mechanical Strength Testing

The mechanical strength such as compressive and hardness testing process for HEO was carried out using a universal testing machine (UTM) and Vickers hardness testing machine (HVS-50) respectively. In a compression test, the material experiences opposing forces that push inward upon the specimen from opposite sides or are otherwise compressed, crushed, or flattened. Then, the result of the test was expressed by the applied compressive load (compressive stress) vs. plastic deformation (compressive strain) and the maximum compressive strength obtained by using maximum applied load divided by the cross-section area of the sintered pellet samples.

The Vickers Hardness test (HVS-50) is used to characterize the hardness of high-entropy oxide pellets. Its measurements were performed with a square diamond pyramid was pressed against the sintered pellets with a 10 kgf load for a holding time of 15 seconds. As a result of the indenter's shape, the impression on the surface of the specimen will be a square and whose opposite sides meet at an angle of 136° is employed in the Vickers hardness test. The length of the diagonal of the square is measured through a microscope fitted with an ocular micrometer. The indentations were examined for conformation with the standard ASTM C1327. Finally, the hardness number can be calculated by the load over the surface area of the indentation. Hardness may vary as a function of load, therefore, it is advised to specify applied when HV hardness is reported. Additionally, microstructure, porosity, and relative density correlated with mechanical strength were investigated by using SEM and Archimedes principles respectively. The relative densities were calculated utilizing theoretical densities computed utilizing an ideal stoichiometry and the lattice parameter measured by XRD.

4. RESULTS AND DISCUSSION

4.1 Structure and Phase Compositions

4.1.1 XRD Analysis of MgO

In this work, the as-synthesized MgO sample is characterized by XRD, to determine phase purity, crystal structure, lattice parameters, and average crystallite size using Scherer's formula. Figure 4.1(**a)** depicts the XRD pattern of as-synthesized MgO sample showing that the phase purity of the sample and the peaks have appeared at angles (2θ) of 36.89°, 42.86°, 62.22°, 74.59°, and 78.52° corresponding to (111), (200), (220), (311), and (222) planes respectively. The obtained information was confirmed to be accurate according to the standard of cubic MgO crystal structure (JCPDS Card No. 45-0946 with a space group of Fm-3m) [102]. Moreover, it is observed that the highest intensity peak is obtained at (200) crystal planes of MgO with the FCC phase (lattice constant of cubic unit cell **a=** 0.422 nm). There is no secondary phase that could be detected in the XRD pattern of MgO; indicating that pure MgO is obtained. The average crystallite size was calculated using the Debye-Scherrer formula, by assuming the spherical crystalline cubic structures.

$$\boldsymbol{D = \frac{k\lambda}{\beta_{hkl}\cos\theta}} \qquad \textbf{(4.1)}$$

Where: **λ** is the wavelength of X-ray diffraction used (1.5406 Å in the present case), k is a particle shape factor (k = 0.94), **β** is the full width in radiation at half-maximum of the peak (FWHM), and **θ** is the Bragg angle of X-ray diffraction peak. The calculated average crystallite size of as-synthesized MgO nanoparticles was 15.70 nm.

4.1.2 XRD Analysis of CoO

The crystal structure of CoO powders as shown in Figure 4.1**b**, all the major peaks of as-synthesized samples can be easily indexed with a rock-salt structure with the space group of Fm-3 m. Diffraction peaks related to impurity are not observed in the XRD patterns, besides confirming the high purity of the synthesized product. The average crystallite size of the CoO nanoparticles calculated using the Debye Scherer formula (according to equation 4.1) was about 51.20 nm. Hence, the obtained results are in good agreement with the previously reported (JCPDS Card No. 48-1719) [103].

4.1.3 XRD Analysis of NiO

The X-ray diffraction patterns of the NiO powders prepared by co-precipitation methods and calcined at 600 ℃ are shown in Figure 4.1**c**. The diffraction peaks of NiO Nano-particles at 2θ values of 37.16°, 43.22°, 62.75°, 75.27°, and 79.24° corresponding to (111), (200), (220), (311) and (222) crystal planes, respectively, were well indexed to FCC crystal structure with lattice constant a= 0.418 nm and space group of Fm-3m (JCPDS Card No. 47-1049) [104]. No additional peaks are corresponding to the secondary phases were detected in the XRD pattern and besides, confirming the high purity of the as-synthesized NiO samples. The average crystallite sizes of the samples calculated by Debye-Scherer's equation (Equation 4.1) using the full width at half maximum of (111), (200), and (220) of the X-ray diffraction peaks was 17.80 nm.

4.1.4 XRD Analysis of CuO

Figure 4.1**d** shows the experimental XRD patterns of as-synthesized CuO nanoparticles measured at room temperature. All XRD peak positions are consistent with standard Copper oxide structures, and identical to pure cubic structure in the monoclinic phase (space group C2/c) of CuO (JCPDS # 48-1548) [105]. The average crystallite size of the as-synthesized product was calculated using the Debye-Scherrer formula (Equation 4.1) was 21.3 nm.

4.1.5 XRD Analysis of ZnO

As shown in Figure 4.1**e**, the obtained XRD results of sample calcined at the temperatures of 500 ℃, exhibits sharp diffraction peaks at angles (2θ) of 31.77°, 34.42°, 36.26°, 47.54°, 56.60°, 62.87°, 66.39°, 67.95°, 69.10°, 72.54° and 76.96° corresponding to (100), (002), (101), (102), (110), (103), (200), (112), (201), (004) and (202) planes respectively. The XRD pattern is well matched with the standard patterns of hexagonal crystal system (Wurtzite structure which has lattice constants a= b= 3.227 and c= 5.417) of ZnO (JCPDS Card No. 36-1451; P63mc) [106]. The average crystallite size of as-synthesized ZnO nanoparticles was estimated using Scherer's equation (Equation 4.1) was 33.9 nm.

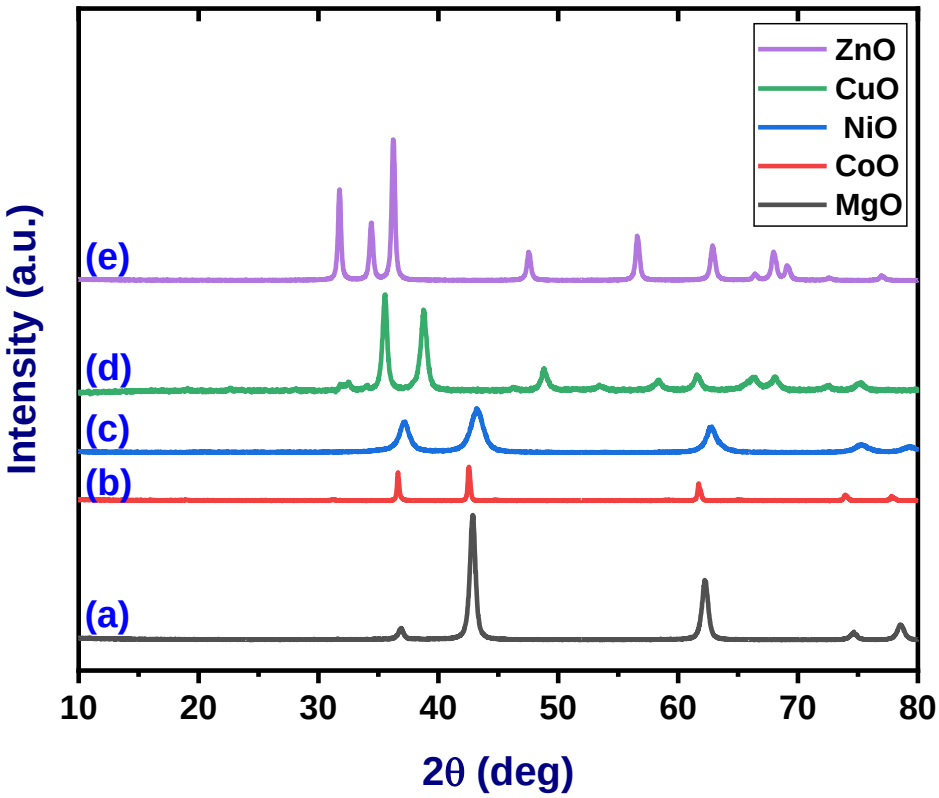

Figure 4.1: *XRD patterns of individual binary Oxides* ***(a)*** *MgO,* ***(b)*** *CoO,* ***(c)*** *NiO,* ***(d)*** *CuO, and* ***(e)*** *ZnO as-synthesized nanoparticles.*

4.1.6 XRD Analysis of HEO

The starting binary oxides used to synthesize the HEO system (MgO, CoO, NiO, CuO, and ZnO) were examined by XRD, thereby, it was confirmed that the five oxides had three different crystal structures [33]. Namely, MgO, CoO, and NiO had the rock-salt structure, whereas, CuO had the tenorite structure, and ZnO had the Wurtzite structure. Moreover, for MgO, CoO, and NiO the crystal structures of the initial and final states are all rock-salt structures. While for CuO and ZnO, there must be a structural transition to the rock-salt crystal phase from the tenorite and Wurtzite phases respectively. Based on the literature [107], reported that the mixing enthalpies ($\Delta H_{\mathbf{mix}}$) of the Wurtzite to rock-salt and tenorite to the rock-salt transformation of ZnO and CuO are 25 and 22 kJ mol^{-1}, respectively. It is also well known that positive $\Delta H_{\mathbf{mix}}$ causes incomplete miscibility which leads to phase segregation at lower temperatures and can be stabilized at elevated temperatures [46, 48]. That is why the presence of tenorite and Wurtzite phases can be detected at low temperatures.

When the increasing of calcination temperature, which leads to the achievement of maximum configurational entropy of the system at optimum temperature; hence, it drove the five oxides to form a single-phase rock-salt crystal structure due to exhibiting randomly distribution of cations in sub-lattices.

The XRD patterns of the samples presented in Figure 4.2 was conducted to verify the structural information of as-synthesized near to equimolar compositions ($Mg_{0.2}$ $Co_{0.2}$ $Ni_{0.2}$ $Cu_{0.2}$ $Zn_{0.2}$)O) nanocrystalline powders are calcined at temperatures ranging from 750 ℃ - 1100 ℃ with 50 ℃ increments. The obtained XRD patterns have shown that, the sequence of single-phase formations of the HEO systems. Moreover, at the lowest temperature regime especially around 750 ℃, the powders did not form a single-phase structure and the different peaks for the individual oxides phases were observed, namely Rock-salt, Tenorite, Wurtzite, and Co_3O_4 spinel structure. Then, the fraction of Wurtzite (ZnO, P63mc), Tenorite (CuO, C2/c), and Co_3O_4-like spinel (Fd-3m) phases were reduced with increasing of calcination temperature to 900 ℃ and above. This phenomenon is due to the partial conversion to the rock-salt phase; and at the same time, the Co_3O_4-like spinel-phase disappears due to its complete decomposition into CoO.

The X-ray diffraction patterns of the major peaks of a sample calcined at 950 ℃ can be easily indexed with a single-phase, rock-salt structure with the space group of Fm-3m (standard XRD patterns of HEO systems) [81]. According to the standardized PDF cards (Figure 4.2), the obtained five major crystal planes of (111), (200), (220), (311) and (222) correspond to 2θ values of 36.80°, 42.75°, 62.01°, 74.31°, and 78.19° respectively, which should be perfectly matched with rock-salt FCC structure [33]. There are no additional peaks corresponding to secondary phases that can be detected in the above-mentioned sample at specific calcination temperatures of 950 ℃, which shows the proper random distribution of cations in the sublattice of the HEO system. Hence, the full conversion to the single-phase rock-salt structure of the system occurs at 950 ℃ (as shown in Figures 4.2 and 4.3). However, the increasing of calcination temperatures (above 1000 ℃) causes a marginal shift of the identified XRD peaks towards higher angle side and the additional minor diffraction peaks (as secondary phases) observed on the sample, which lied at around 2θ = 62.20°; as shown in Figure 4.3**b**. Similarly, it is observed that at lower calcination temperatures almost all peaks were shifted into higher 2**θ** values (as shown in Figure 4.3**a**&**b**).

This phenomenon may be due to immiscibility and altering of cations in sub-lattices, which leads to the reverse phase transformation of the systems; and it assures the other researcher's results who reported on the reversible phase transition of HEO [44]. Additionally, it indicates that the increment of average crystallite size (according to equation 4.1, D= 58.940 nm at elevated temperature) and leads to somewhat inhibiting randomly distributions of cations in the sublattice. At the temperature between 900 ℃ - 1000 ℃, the peaks were almost shifted to lower angles of 2**θ** values, and which shows a decrease of average crystallite sizes of the samples (D= 50.936 nm) which is used to facilitate randomly distribution of cations in their sub-lattices. Notably, all the experimental data obtained specifically at 950 ℃ were well matched with the calculated data for rock-salt structure, indicating a good fit. The calculated lattice constant and crystallite size are 0.4218 nm, 50.936 nm, respectively.

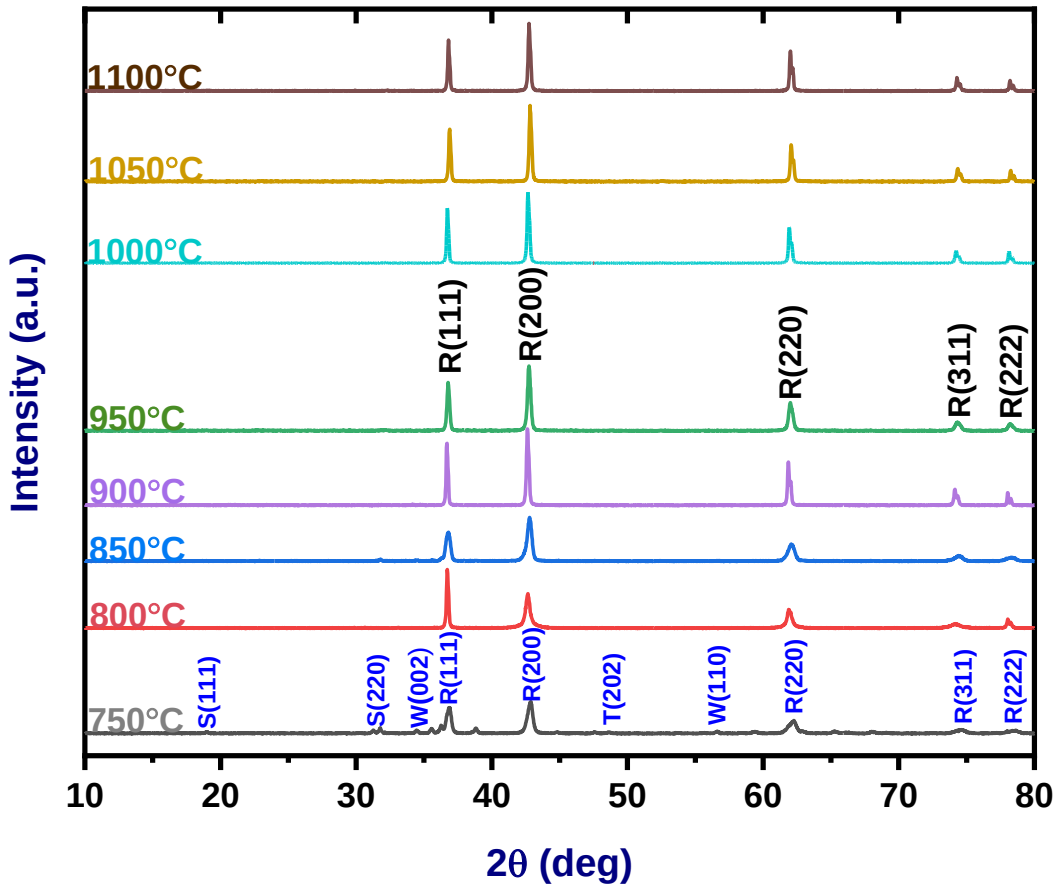

Figure 4.2: *XRD patterns for the entropy-stabilized oxide of an equimolar mixture of MgO, CoO, NiO, CuO, and ZnO. The patterns were collected from the powder form of mixture calcined at the temperature range of 750 ℃ – 1100 ℃ with 50 ℃ increments; indicated structures of Rock salt (R), Wurtzite (W), Tenorite (T), and Co3O4 spinel (S).*

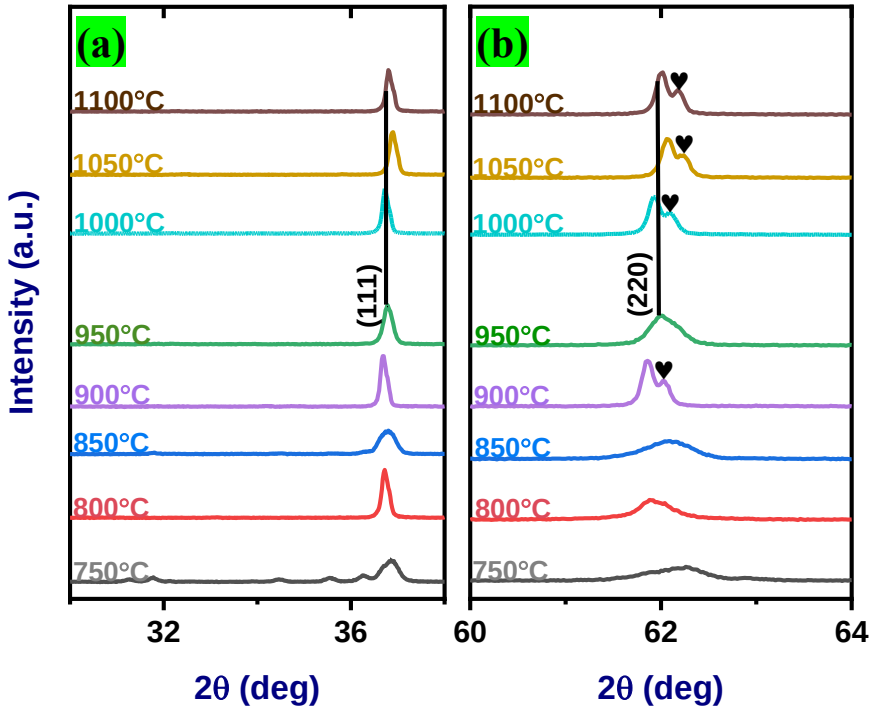

Figure 4.3: *XRD pattern of HEO system for expansion of the diffraction peaks of* ***(a)*** *(111) from 2θ of 30°– 40° and* ***(b)*** *(220) from 2θ of 60°– 64°; the Copyright signs identify minor secondary phases.*

4.1.7 Phase-Stability upon Heat Treatment and Configurational Entropy Effects

The effect of entropy on single-phase stabilization of HEO pellets was characterized by heat treatment of (Mg-Co-Ni-Cu-Zn)O system at the temperature ranges of 900 ℃ - 1200 ℃ with 100 ℃ increments, followed by air cooling to room temperature. The obtained pellet is milled into a fine powder and the phase stability was characterized using XRD. Figure 4.4(**a**–**c**) shown that, the X-ray diffraction patterns of as ball-milled powder, calcined powder, and sintered pellets; all peaks of the individual oxides with their structures are displayed in Figure 4.4**a**. Besides, the results have shown that a pure single-phase of HEO was obtained from the pellets sintered at 1200 ℃ which was well matched with powder calcined at 950 ℃. The obtained peaks of HEO pellet and powder had a typical face-centered cubic (FCC) structure with the position of their diffraction peaks that were almost identical and no phase separation was observed (Figure 4.4 **b** and **c**). Moreover, the summary of results obtained by Rietveld refinement of the samples along with the space group of their main phase and formation of a single-phase were well indexed with the standard XRD pattern of HEO systems [81].

Additionally, based on the effect of entropy on the phase-stability of the system; the obtained results of calculated maximum configurational entropy (ΔS_{config}) value of as-synthesized HEO in an equiatomic 5-cations system was 1.61 *R* per mole (ΔS_{config} = 1.61 *R*, according to equation 2.1). This result is also consistent with other researcher's results; who reported the effects of configurational entropy in solid solutions of HEO as a function of mole fractions of N^{th} components [15, 44]. These reflections can be indicated that the configurational entropies in the cation sublattice have higher contributions to the successful formation of a single-phase HEO (Mg-Co-Ni-Cu-Zn)O system.

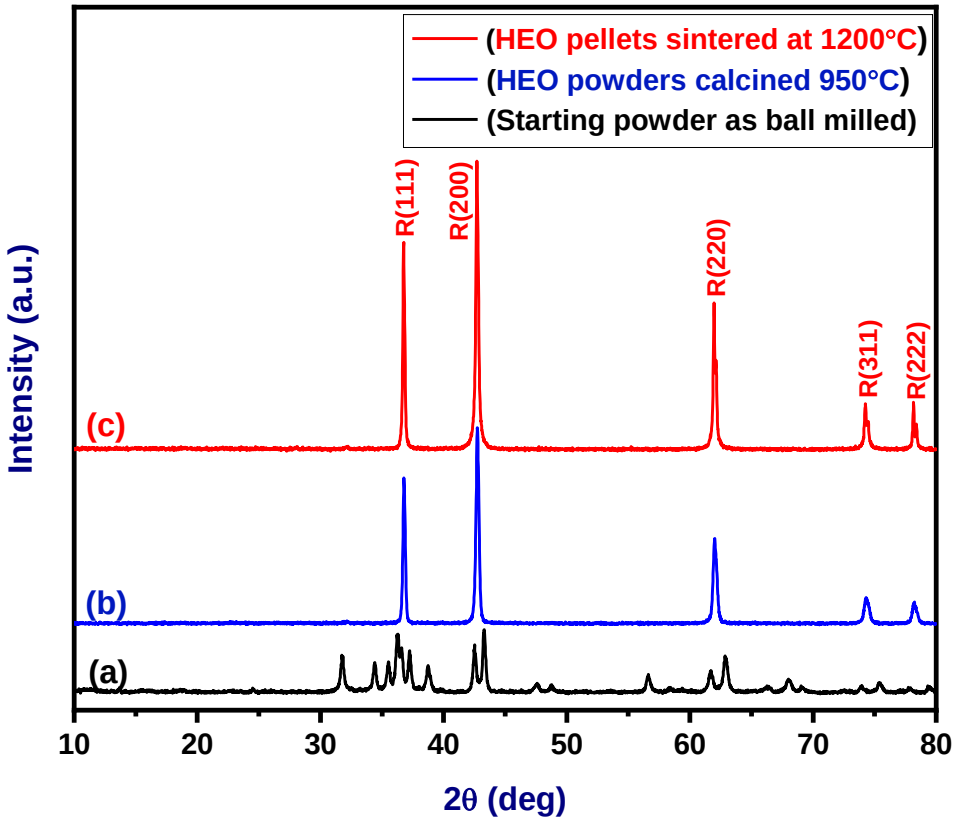

Figure 4.4: *XRD patterns of (**a**) as ball-milled (BM) powder, (**b**) HEO powder calcined at 950 ℃, and (**c**) HEO pellet sintered at 1200 ℃.*

4.2 Microstructural Evolution and Elemental Composition Analysis of High-Entropy Oxide

The mechanical properties of HEO ceramics depend on their microstructure, which is defined by the grain size, morphology, distribution, porosity, and composition of the phases present and by the interface between the grains [108].

In order to improve the properties of ceramics for either structural or functional applications, reducing the grain size and limiting the formation of defects is important. Hence, the microstructural analysis on the free surface of as-synthesized pellets with various sintering temperatures and times was investigated by using SEM.

4.2.1 The Effects of Sintering Temperature

The sintering temperature had a dramatic effect on the final density and mechanical properties of fired pellets of HEO systems. Figure 4.5(**a–d**) shows the SEM images (microstructures) of as-synthesized (Mg-Co-Ni-Cu-Zn)O pellets sintered at a temperature of 900 ℃, 1000 ℃, 1100 ℃, and 1200 ℃ sequentially, for a constant sintering time of 3 h. The SEM images of the samples sintered at 900 ℃ exhibits the presence of spherical-shaped agglomerates containing relatively fine grains with less dense agglomerated particles (Figure 4.5**a**). Several voids (porosities) were existed in the specimen, due to the presence of a loose connection between the grains in this sample. These voids and small flaws were reduced with the increasing temperature; which indicating that, a formation of a better connection between the grains (Figure 4.5**a–d**). However, the grains tend to gradually grow up larger as the sintering temperature progresses and a continuous grain structure is formed due to grain coarsening when sintering temperature increased from 1000 to 1200 ℃. As Figure 4.5**d** shown that, the surface diffusion of the samples sintered at 1200 ℃ is enhanced and promotes the preferential neck growth with a certain increase in density and reduction of porosities. Besides, the density of samples was increased and becoming initiate to form a grain boundary. However, the porous surface was observed on the samples, due to the process that occurred by using low sintering times (3 h). The effect of sintering temperature on the synthesized (Mg-Co-Ni-Cu-Zn)O system is summarized in Table 4.2 and shown graphically in Figure 4.8.

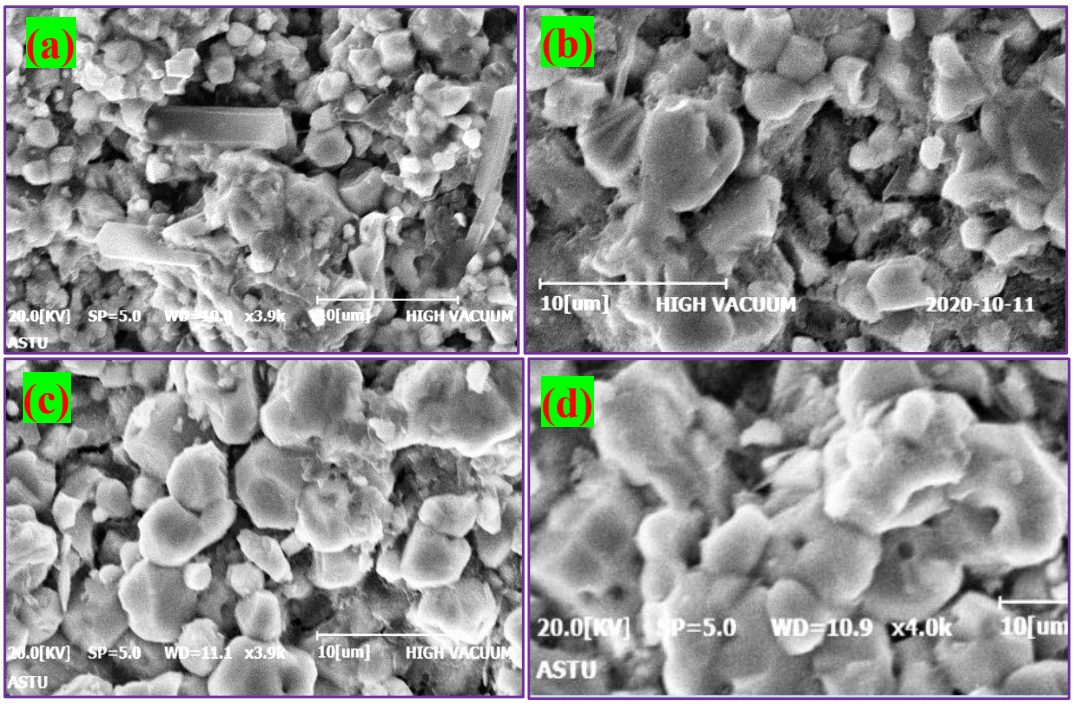

Figure 4.5: *SEM images of HEO pellets sintered at the temperature of* ***(a)*** *900 ℃,* ***(b)*** *1000 ℃,* ***(c)*** *1100 ℃,* ***(d)*** *1200 ℃, for constant sintering time of 3 h.*

4.2.2 The Effects of Sintering Temperature with Time

The effect of sintering temperatures with sintering time can be also determined based on microstructural changes, mainly coming from the enhancement of the densification due to the reduction of porosities, which has a huge impact on the final properties of a sintered ceramics. As shown in Figure 4.6(**a–d**), the fully densified structures were observed due to the sequentially increasing firing temperatures and times. Hence, the micrographs reported in Figure 4.6 reveal a very dense microstructure with small pores, mainly located at the grain boundary. An increase in the sintering time from 3 to 15 h at 1100 ℃ and 1200 ℃, increased the relative density by approximately 16%, and 19% respectively (shown in Table 4.3, Figures 4.9 and 4.10). Besides, the density measurements are in agreement with the microstructural analysis, the relative density being close to 99.2% for a sample sintered at 1200 ℃ for 15 h. The average grain sizes were gradually increased with increasing the sintering time and temperatures (Figure 4.6**a–d**). Especially, it is broader at the sintering temperature of 1200 °C. This phenomenon might directly affect the mechanical properties of materials, due to providing the relatively free movement of dislocations along the grain boundary and producing a high probability to initiate the crack propagation of the systems.

The energy dispersive X-ray (EDX) spectroscopy, the elemental analysis of as-synthesized (Mg-Co-Ni-Cu-Zn)O pellets clearly shows, the peaks of elements for O, Co, Ni, Cu, Mg, and Zn, all were present in the samples of the HEO system (Figure 4.6**e**). Moreover, the obtained result confirms that the HEO system contains transition metallic oxides in near to equiatomic amounts as desired and expected form of single-phase solid solutions, that as confirmed through by XRD.

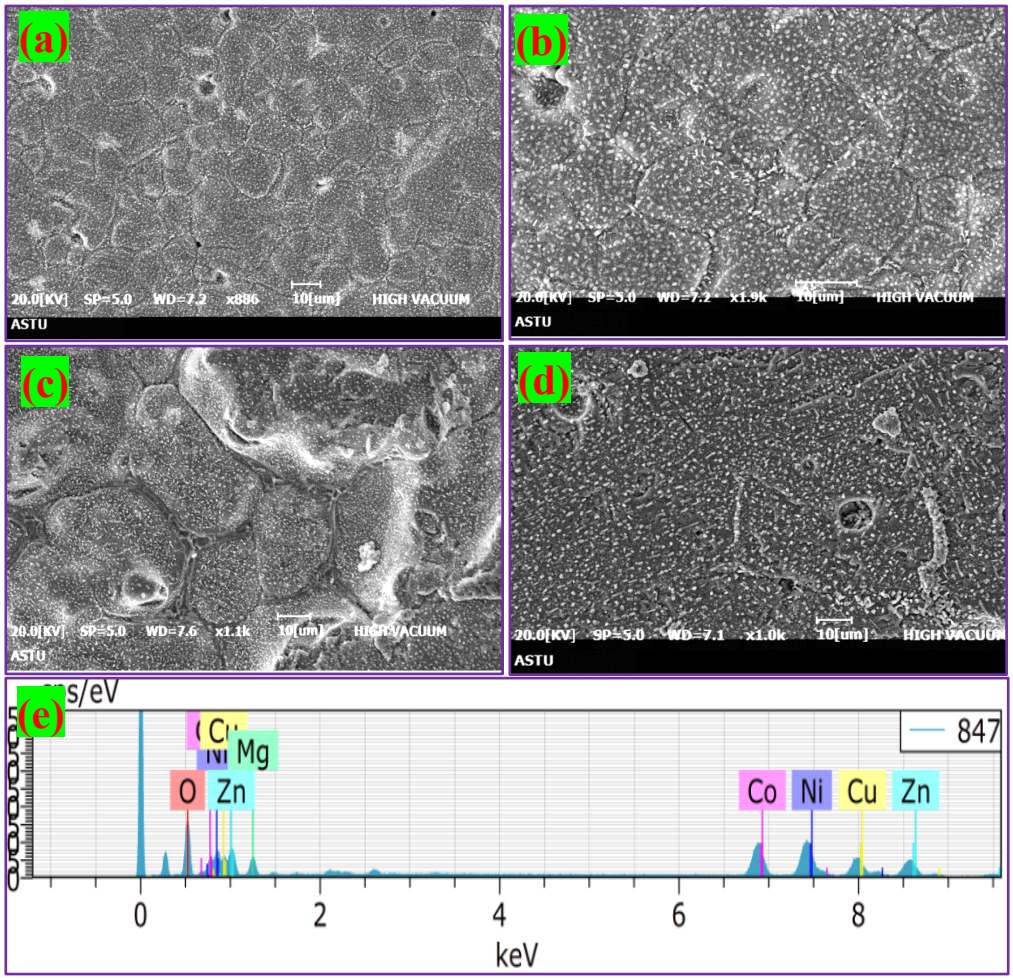

Figure 4.6: *SEM images of HEO pellets sintered at the temperature of* ***(a)*** *1100 ℃ for 9 h,* ***(b)*** *1100 ℃ for 15 h,* ***(c)*** *1200 ℃ for 9 h,* ***(d)*** *1200 ℃ for 15 h, and* ***(e)*** *EDX analysis of HEO systems.*

4.3 Thermal and Phase-Stability of Pre-alloyed HEO Powders

The thermo-gravimetric analysis was conducted on an instrument referred to as a Thermo-gravimetric analyzer and the experiment consisted of registering the weight loss of the sample as a function of temperature.

The thermal behavior of pre-alloyed powders of the HEO system is shown below in Figure 4.7. The TG-DTA plots for the powder form of the sample were characterized by three main endothermic peaks of thermal effects (indicated as **α**, **β**, and **δ**) and three exothermic peaks (indicated **a, b,** and **c**). Especially, the three endothermic peaks of decompositions were more related with the weight losses of the samples. Thereby, the first thermal effect (**α**) for pre-alloyed powder takes place at about (~78.51 ℃) and corresponds to endothermic peaks paired with consistent weight losses, about (~24.60 wt%). The origin of the "**α**" effect is very likely the evaporation of residual water and moisture from the surface of the samples.

The second effect "**β**" transformation of endothermic peaks takes place within the temperatures of around (~286.26 ℃), where hydroxides and basic carbonates of the different metals used in this work typically decompose [109]. Besides, it is likely associated with the removal of their crystallization water and carbon dioxide (about weight losses of ~17.59%). In the third step decomposition "**δ**" a pronounced endothermic peak is observed around the temperature of (~743.56 ℃) with a consistent weight loss of about ~0.25 %. The weight loss resulted from the decomposition of Co_3O_4 to CoO with the simultaneous evolution of O_2 to maintain stoichiometry [110, 111]. As a result of these three steps of decompositions 41.862%, total mass loss is observed on the TG-DTA curves. This loss may be attributed to the combination of multicomponent of the HEO system with their own decomposition behaviors.

Finally, the three exothermic peaks (**a**, **b**, & **c**) can be observed in pre-alloyed powder, not paired with any weight change in the TGA plot. Moreover, it is interesting to observe that around 950 ℃, the system is already largely composed of the rock-salt structure typical of (Mg-Co-Ni-Cu-Zn)O entropy-stabilized oxide. As seen in Figure 4.7, there is no considerable loss of weight was observed from the samples above 900 ℃ and the TG-DTA curve reveals the thermal and phase-stability of the HEO system. It assures that, the formation of stable and single-phase structure was achieved at the optimum temperature of the systems.

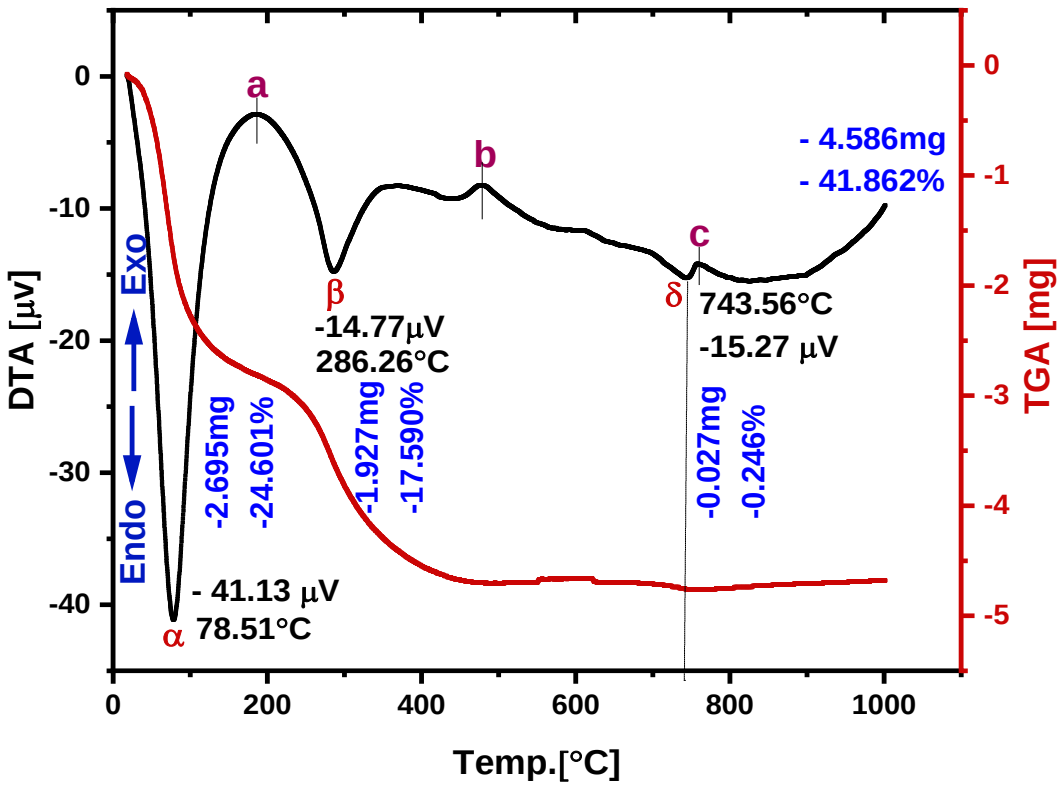

Figure 4.7: *TG-DTA plots of pre-alloyed high entropy oxide powders.*

4.4 Physico-Mechanical Properties of High-Entropy Oxide

Many ceramics undergo a significant increase in density during sintering which is a critical issue for developing desirable properties such as mechanical strength. Besides, reducing the grain size and limiting the formation of defects is one of the important parameters to enhance the mechanical properties of ceramic materials for structural applications. During the sintering period, considerable microstructural development, densifications, and grain growth take place; which is controlled by the sintering temperatures and times [112]. Accordingly, the density of sintered pellet specimens was measured through the Archimedes' principle in water immersion and by using an analytical balance [113, 114]. The measures were repeated on two (2) different samples per each sintering temperature with sintering times (totally 16 samples). Based on the Archimedes procedures, the pellets were weighed as dry (M_a), and then saturated with water and the suspended weight (M_w) was measured by hanging a saturated pellet from the balance into water. Consequently, the saturated weight (M_s) was measured by removing a pellet from the saturating liquid, lightly wiping it to remove excess water from the surface, then quickly transferring it to the balance.

Finally, the pellet densities were calculated after sintering (sintered density ρ_s), in water using the Archimedes principle as follows:

$$\rho_s = \frac{Ma}{(Ms-Mw)\rho_w} (g/cm^3) \quad (4.2)$$

Where: M_a is the mass of the sample in the air; M_s is the mass of the sample in the air after submerged in water; M_w is the mass of the sample in water; ρ_w is the density of water (1 g/cm^3), and ρ_s is the sintered density. Based on the above procedures and equation the measured dry weight of sintered samples (with a standard deviation of ±0.125), suspended weights, saturated weights, and calculated density values of sintered pellets with different temperatures and sintering times were listed in Table 4.1.

Table 4.1: *Measured weight and calculated density of sintered pellets of the HEO system with different sintering temperatures and times.*

Sintering Temperature (°C)	Sintering Time (h)	Dry Weight, M_a (g)	Suspended Weight, M_w (g)	Saturated Weight, M_s (g)	Sintered Density, ρ_s (g/cm^3)
900	3	2.901	2.510	3.189	4.272
1000	3	2.794	2.526	3.115	4.774
1100	3	2.845	2.515	3.105	4.822
1200	3	2.594	2.399	2.915	5.027
1100	9	2.795	2.411	2.913	5.568
1100	15	2.842	2.526	3.016	5.800
1200	9	2.590	1.995	2.430	5.954
1200	15	2.899	2.657	3.131	6.116

As the results have shown, with increasing sintering temperature from 900 to 1200 °C with 100 °C increments), and sintering times (3-15 h with 6 h intervals) the density of sintered pellets was increased. These phenomena may have occurred, due to the removal of porosity and improvement of an inter-granular bonding. Thereby, it leads to the enhancement of mechanical properties, such as compressive strength and hardness values of (Mg-Co-Ni-Cu-Zn)O sintered pellets.

To calculate the relative density of the samples, firstly the theoretical density **(ρ_t)**, based on an idealized uniform dispersion of metallic oxides in sublattice sites, of HEO specimens were calculated for all solid solutions using their lattice parameters from the diffraction patterns. The theoretical density and relative density (ρ_s (%)) of as-synthesized pellets were computed via Equations (4.3) and (4.4) respectively.

$$\rho_t = \frac{Cell\ Mass}{Cell\ Volume} = \frac{n*Mwt}{Vc*N} = \frac{n*Mwt}{(a)^3*N}\ \ (g/cm^3) \qquad (4.3)$$

Where: n is the number of atoms per unit cell; Mwt is the molecular weight of the compound; N is the Avogadro's number, and a = b = c are the lattice parameters of the Rock-salt structure of the sample obtained by XRD from the powder diffraction data.

$$\rho_s(\%) = \left(\frac{\rho_s}{\rho_t}\right) x\ 100 \qquad (4.4)$$

The calculated result of theoretical density was ρ_t = 6.166 g/cm^3 (according to equation 4.3). The results of calculated relative densities (according to equation 4.4) are expressed in percentages were listed in Tables 4.2 and 4.3; it is confirmed that the densities increased with increasing sintering temperatures and times.

The compressive strength and Vickers hardness of as-synthesized pellets of HEO systems with different sintering temperatures (900 ℃, 1000 ℃, 1100 ℃, and 1200 ℃) and similarly variation of temperature with sintering times are listed in Table 4.2 and 4.3. To obtain the results of mechanical strength, a total eight (8) specimens were prepared for each sintering temperature with time from the proposed materials to show the comparisons of the test results according to their parameters. The compression test was carried out by using the applied maximum loads of (26.50 - 49.01 KN) for the samples sintered at the temperatures of (900-1200 ℃) with a sintering time of (3-15 h). The obtained result of compressive strength and hardness values were calculated from measured values of the specimens by using the equation 4.5 and 4.6 respectively.

$$F = P/A \qquad (4.5)$$

Where: F is the compressive strength of the specimen (in MPa). P is the maximum load applied to the specimen (in KN) and A is the cross-sectional area of the specimen (in mm^2).

Similarly, the hardness values were measured and calculated using equation 4.6.

$$HV = 1.8544F/D^2 \qquad (4.6)$$

Where: F is the applied load measured in kilograms-force (kgf) and D is the mean diagonals of impression (mm).

Table 4.2: *Comparison of Relative density and mechanical properties for HEOs with different sintering temperatures at constant sintering times (3 h).*

Sintering Temperature (°C)	Relative Density (%)	Compressive Strength (MPa)	Vickers Hardness (MPa)
900	69.28	99.36	1294.79
1000	75.94	124.08	1544.36
1100	78.20	139.06	1602.97
1200	80.53	163.46	1799.89

The obtained data of compression strength and hardness value were collected from the HEO pellets samples sintered at various temperatures and times. Thereby, the obtained results have shown that with increasing sintering temperature the compressive strength, relative densities, and harness value of samples were increased (as shown in Figure 4.8).

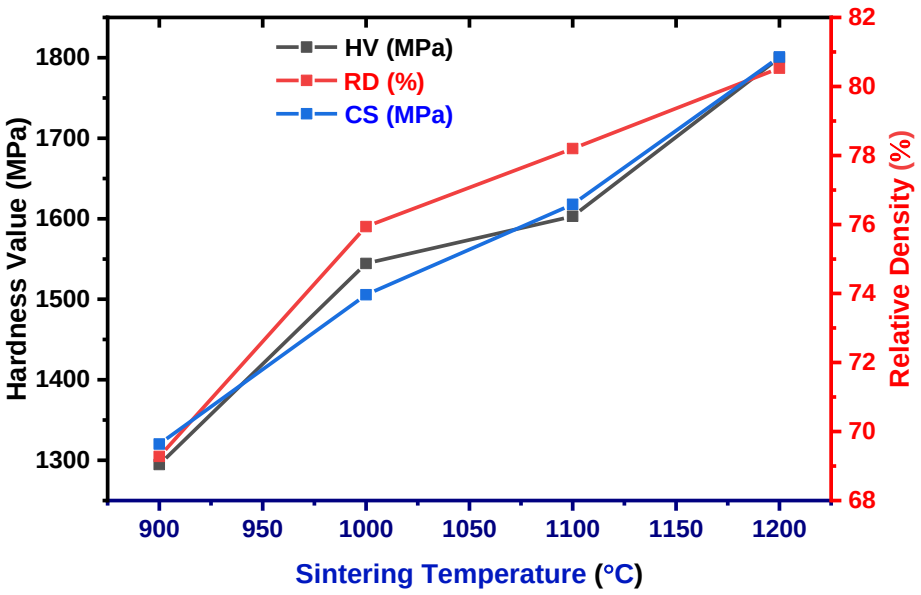

Figure 4.8: *Result of Hardness, Compressive, and Relative Density as a function of sintering temperature at constant sintering time (3 h) for HEO pellets.*

The effect of sintering temperature on the ceramic properties, such as relative density and mechanical strength were examined in specific sintering temperatures of 1100 ℃ and 1200 ℃. The results also showed that the samples were more fully densified (relative density of 99.2%) at the sintering temperatures of 1200 ℃ for 15 h (as listed in Table 4.3). This result also consistent with the other researcher's results which reported on the relative density of high entropy oxides synthesized through field-assisted sintering techniques (FAST) [100]. Especially, in the case of increasing temperature with sintering time, the improvement of mechanical strength was obtained due to the reduction or closed-up of porosity (as shown in Table 4.3 and Figure 4.6**a-d**). Moreover, when porosity decrease, the cohesion between grains was increased; this results in enhancement of relative densities and mechanical strength.

Table 4.3: *Comparison of Relative density and mechanical properties for HEOs with different sintering temperatures and times.*

Sintering Temperature (℃)	**Sintering Times (h)**	**Relative Density (%)**	**Compressive Strength (MPa)**	**Vickers Hardness (MPa)**
1100	9	90.30	220.75	8513.78
	15	94.10	233.51	10277.50
1200	9	96.56	268.20	12448.00
	15	99.20	270.09	15078.26

The increasing relative density was accompanied by a reduction of the open porosity of pellets. Besides, it provides a high probability for enhancement of mechanical properties including compression strength and hardness, due to the improvement of intergranular bonding. Hence, as Figures 4.9 and 4.10 were shown that, the improvement of mechanical strength and relative densities of as-synthesized samples were observed through sintering processes.

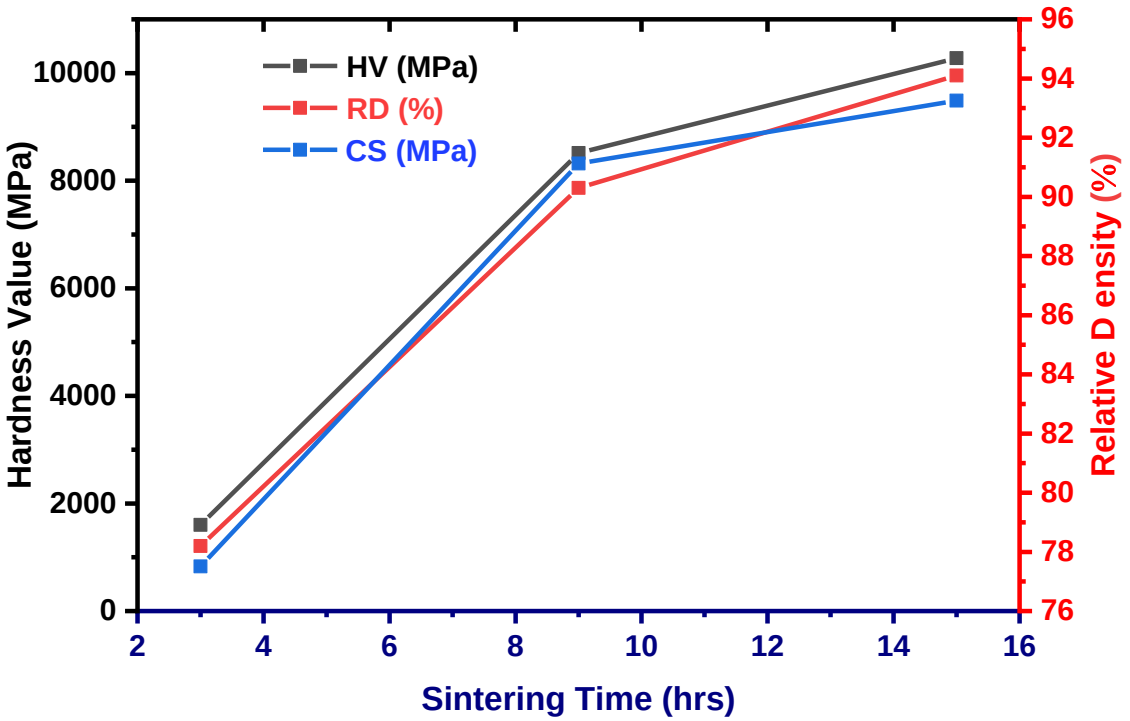

Figure 4.9: *Result of Hardness, Compressive, and Relative Density as a function of sintering time at a constant sintering temperature (1100 ℃) for HEO pellets.*

The measured results of Vickers hardness values (HV) of sintered pellet specimens were in the range of 1.3 to 15.1 GPa in various sintering temperatures and times (as listed in Table 4.2 and 4.3). Specifically, the samples sintered at the temperatures of 1100 ℃ and 1200 ℃ for sintering times of 9 h and 15 h, which possess significantly higher hardness values of 8.5-15.1 GPa (as listed in Table 4.3). Besides, the obtained result was more comparable with that of another researcher [115], who reported hardness values of high entropy fluorite oxide ceramics varies from 12.3 to 15.6 GPa. Finally, the effect of sintering temperature with sintering times on HEO systems is summarized in Table 4.3 and shown graphically in Figures 4.9 and 4.10.

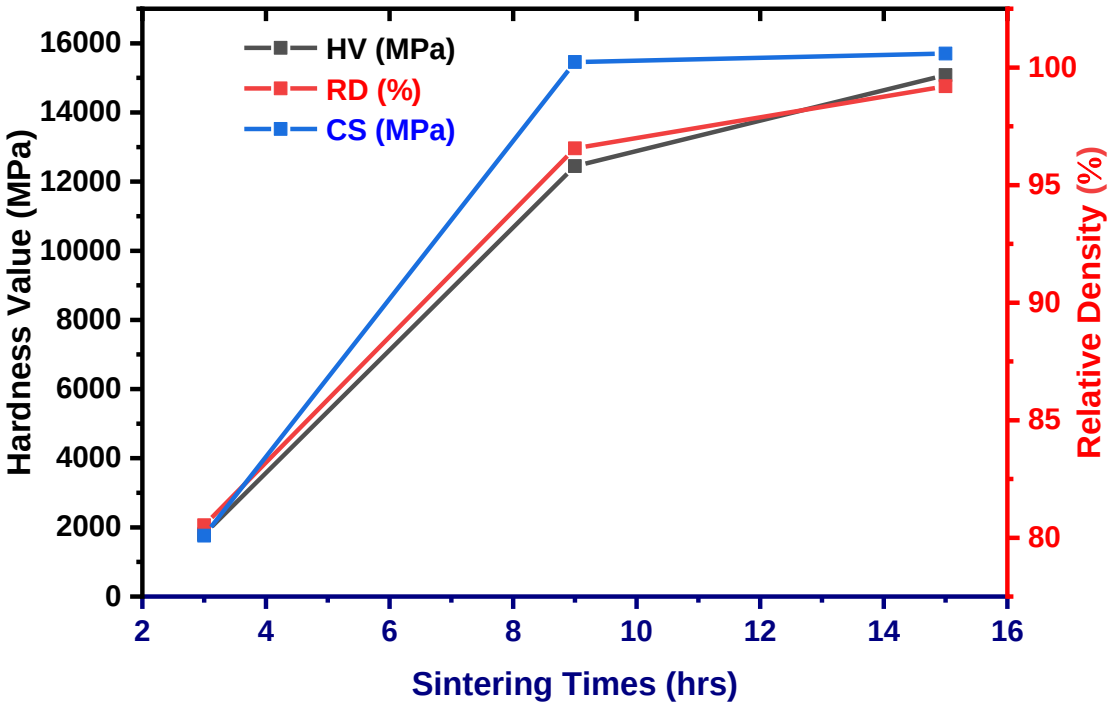

Figure 4.10: *Result of Hardness, Compressive, and Relative Density as a function of sintering time at a constant sintering temperature (1200 ℃) for HEO pellets.*

As shown in Figure 4.10, the sample sintered at 1200 ℃ for 15 h showed a maximum compressive strength and Vickers hardness of about 270.09 MPa and 15.10 GPa, respectively, with a corresponding relative density of about 99.20%.

5. CONCLUSION AND RECOMMENDATIONS

5.1 Conclusion

In the present work, all individual metallic oxides (MgO, CoO, NiO, CuO, and ZnO) were successfully synthesized through co-precipitation methods. The XRD analysis confirmed that the highly pure phases of binary oxides were obtained. The multicomponent HEO (Mg-Co-Ni-Cu-Zn)O was successfully synthesized by using obtained binary oxides as a precursor through conventional solid-state reaction methods. The phase stability and compositional analysis were characterized using XRD and SEM+EDX. The XRD results confirmed that as-synthesized HEO exhibit a single-phase with high compositional uniformity at optimum temperature. Consequently, the EDX analysis assured that the elements of O, Co, Ni, Cu, Mg, and Zn were present in the HEO systems. Furthermore, we also studied the effect of calcination temperature and configurational entropy on the formation of a single-phase. Thereby, the pure single-phase rock-salt structure with the space group of Fm-3m occurs at 950 ℃, and the obtained five major peaks were perfectly matched with standard XRD patterns of HEO systems [81]. Also, the thermal and phase stability of as-synthesized HEO either in powder or pellet samples were investigated. Thereby, the HEO powders exhibit a pure single-phase when the sample calcined at 950 ℃ and also still retain as a single-phase structure in case of pellet sintered at 1200 ℃. Besides, the TG-DTA curve confirmed that, the phase stability of the HEO system obtained above 900 ℃. Additionally, the calculated maximum ΔS_{config} value of the as-synthesized equiatomic 5-cations system was 1.61 R per mole; which indicates that the configurational entropy contribution plays a significant role in the formation of single-phase HEO systems. Finally, the mechanical properties such as compressive strength and hardness tests which are directly correlated with microstructure are performed on the sintered samples of HEO using compression and Vickers hardness testing machines. The sample sintered at 1200 ℃ for 15 h showed a fully densified microstructure, a maximum compressive strength, and Vickers hardness of about 270.09 MPa and 15.10 GPa, respectively, with a corresponding relative density of about 99.20%. Hence, these single-phase HEOs have shown exploring properties as high thermal stable materials; and they could be a potential candidate for structural applications. Accordingly, this work will play a significant role by providing options of materials for structural applications.

5.2 Recommendations

- From the mechanical strength point of view, by applying other tests that are not performed in this research works such as wear and impact test to verify the HEO materials for specific structural applications. Additionally, providing the mechanism for controlling grain growth of sintered pellets, which is a very critical issue for the enhancement of mechanical properties of HEO ceramics.
- It is recommended that on the synthesis of HEO pellets; applying optimization of sintering temperature and times with 50 °C increments and 1 h intervals respectively and performing sintering processes of the samples above 1200°C. The effects of sintering temperature and times are very important points to studies the microstructural evolution and mechanical strength of HEO materials.
- It is recommended to use other synthesis methods that are not performed in this work, such as hydrothermal and spark plasma sintering methods, which are very important to control the particle size and to obtain fully densified microstructure in relatively low sintering temperatures. Additionally, by applying further characterization such as TEM for more detailed morphological analysis and determining the particle size of the samples, and XPS for detailed elemental analysis with their oxidation number. Then, investigating the electrical properties of high entropy oxides for different applications.

REFERENCES

1. Huang, Y.a., HEOx---electrical-measurements. 2004.
2. Yeh, J.W., et al., High-Entropy Alloys – A New Era of Exploitation. Materials Science Forum, 2007. 560: p. 1-9.
3. Miracle, D., et al., Exploration and Development of High Entropy Alloys for Structural Applications. High-Entropy, 2014. 16(1): p. 494-525.
4. Zhang, Y., High-Entropy Materials. Springer Nature Singapore Pte Ltd, 2019. 2: p. 215-232.
5. Yeh, J.-Wei., Overview of high-entropy alloys. High-Entropy Alloys. Springer, Cham, 2016. 3: p. 1-19.
6. Yeh, J.-W., et al., Nanostructured High-Entropy Alloys with Multiple Principal Elements: Novel Alloy Design Concepts and Outcomes. Advanced Engineering Materials, 2004. 6(5): p. 299-303.
7. Miracle, D.B. and O.N. Senkov, A critical review of high entropy alloys and related concepts. Acta Materialia, 2017. 122: p. 448-511.
8. Rost, C.M., et al., Entropy-stabilized oxides. Nat Commun, 2015. 6: p. 8485.
9. Dusza, J., et al., Microstructure of (Hf-Ta-Zr-Nb)C high-entropy carbide at the micro and nano/atomic level. Journal of the European Ceramic Society, 2018. 38(12): p. 4303-4307.
10. Tsai, D.-C., et al., Structural morphology and characterization of (Al-Cr-Mo-Ta-Ti) N coating deposited via magnetron sputtering. Journal of Applied Surface Science, 2013. 282: p. 789-797.
11. Guan, J., et al., Synthesis and thermal stability of novel high-entropy metal boron carbonitride ceramic powders. Journal of the Ceramics International, 2020. 46(17): p. 26581-26589.
12. Braic, V., et al., Nanostructured multi-element (Ti-Zr-Nb-Hf-Ta)N and (Ti-Zr-Nb-Hf-Ta)C hard coatings. Surface and Coatings Technology, 2012. 211: p. 117-121.
13. Zhang, R.-Z. and M.J. Reece, Review of high entropy ceramics: design, synthesis, structure, and properties. Journal of Materials Chemistry A, 2019. 7(39): p. 22148-22162.
14. Sarkar, A., et al., Rare earth and transition metal-based entropy-stabilized perovskite-type oxides. Journal of the European Ceramic Society, 2018. 38(5): p. 2318-2327.

15. Sarkar, A., et al., High-Entropy Oxides: Fundamental Aspects and Electrochemical Properties. Adv Mater, 2019. 31(26): p. 1806236.
16. Dupuy, A., X. Wang, and J. Schoenung, Entropic phase transformation in nanocrystalline high entropy oxides. Materials Research Letters, 2019. 7: p. 60-67.
17. Zhang, Y., et al., Microstructures and properties of high-entropy alloys. Progress in Materials Science, 2014. 61: p. 1-93.
18. Sarkar, A., B. Breitung, and H. Hahn, High entropy oxides: The role of entropy, enthalpy and synergy. Scripta Materialia, 2020. 187: p. 43-48.
19. Musicó, B.L., et al., The emergent field of high entropy oxides: Design, prospects, challenges, and opportunities for tailoring material properties. Journal of APL Materials, 2020. 8(4): p. 040912.
20. Yeh, J.-W. and S.-J. Lin, Breakthrough applications of high-entropy materials. Journal of Materials Research, 2018. 33(19): p. 3129-3137.
21. Wang, J., et al., Spinel to Rock-Salt Transformation in High Entropy Oxides with Li Incorporation. Journal of Electrochem, 2020. 1(1): p. 60-74.
22. Manzoor, A., et al., Entropy contributions to phase stability in binary random solid solutions. npj Computational Materials, 2018. 4(1): p.1-10.
23. Wang, Q., et al., High entropy oxides as anode material for Li-ion battery applications: A practical approach. Journal of Electrochemistry Communications, 2019. 100: p. 121-125.
24. Zhang, R.Z., et al., Data-Driven Design of Ecofriendly Thermoelectric High-Entropy Sulfides. Inorg Chem, 2018. 57(20): p. 13027-13033.
25. Sarkar, A., et al., Nanocrystalline multicomponent entropy stabilized transition metal oxides. J. Eur. Ceram. Soc., 2017. 37(1): p. 723-734.
26. Zhao, Z., et al., (Ti-Zr-Hf)P_2O_7: An equimolar multicomponent or high entropy ceramic with good thermal stability and low thermal conductivity. Journal of Materials Science & Technology, 2019. 35(10): p. 2227-2231.
27. Zhou, J., et al., High-entropy carbide: A novel class of multicomponent ceramics. Ceramics International, 2018. 44(17): p. 22014-22018.
28. Biesuz, M., et al., High entropy $Sr((Zr_{0.9}4Y_{0.06})_{0.2}Sn_{0.2}Ti_{0.2}Hf_{0.2}Mn_{0.2})O_{3-x}$ perovskite synthesis by reactive spark plasma sintering. Journal of Asian Ceramic Societies, 2019. 7(2): p. 127-132.
29. Sarkar, A., et al., High entropy oxides for reversible energy storage. Nat Commun, 2018. 9(1): p. 3400.

30. Chen, K., et al., A five-component entropy-stabilized fluorite oxide. Journal of the European Ceramic Society, 2018. 38(11): p. 4161-4164.
31. Pickering, E.J. and N.G. Jones, High-entropy alloys: a critical assessment of their founding principles and future prospects. Journal of International Materials Reviews, 2016. 61(3): p. 183-202.
32. Parida, T., et al., Novel rare-earth and transition metal-based entropy stabilized oxides with spinel structure. Scripta Materialia, 2020. 178: p. 513-517.
33. Sarkar, A., et al., Nanocrystalline multicomponent entropy stabilized transition metal oxides. Journal of the European Ceramic Society, 2017. 37(2): p. 747-754.
34. Zhong, Y., et al., Exploration of high entropy ceramics (HECs) with computational thermodynamics - A case study with $LaMnO_{3\pm\delta}$. Journal of Materials & Design, 2019. 182: p. 108060.
35. Djenadic, R., et al., Multicomponent equiatomic rare earth oxides. Materials Research Letters, 2016. 5(2): p. 102-109.
36. Wang, Z., et al., Atomic-size effect and solid solubility of multicomponent alloys. Scripta Materialia, 2015. 94: p. 28-31.
37. Bates, C.H., W.B. White, and R. Roy, The solubility of transition metal oxides in zinc oxide and the reflectance spectra of Mn^{2+} and Fe^{2+} in tetrahedral fields. Journal of Inorganic and Nuclear Chemistry, 1966. 28(2): p. 397-405.
38. Kenny, D.S. and A. Navrotsky, Approximate activity-composition relations in the system MgO and ZnO at 1205±5°C. Journal of Inorganic and Nuclear Chemistry, 1972. 34(7): p. 2115-2119.
39. Rustad, J.R., Density functional calculations of the enthalpies of formation of rare-earth orthophosphates. American Mineralogist, 2012. 97(5-6): p. 791-799.
40. Shannon, R.D., Revised effective ionic radii and systematic studies of interatomic distances in halides and chalcogenides. Acta Crystallographica Section A, 1976. 32(5): p. 751-767.
41. Liu, H., J.S. Tse, and H.-k. Mao, Stability of rocksalt phase of zinc oxide under strong compression: Synchrotron x-ray diffraction experiments and first-principles calculation studies. Journal of Applied Physics, 2006. 100(9): p. 093509.
42. Grzesik, Z., et al., Defect structure and transport properties in (Co, Cu, Mg, Ni, Zn)O high-entropy oxide. Journal of the European Ceramic Society, 2019. 39(14): p. 4292-4298.

43. Stygar, M., et al., Formation and properties of high entropy oxides in (Co-Cr-Fe-Mg-Mn-Ni)O system: Novel (Cr-Fe-Mg-Mn-Ni)$3O_4$ and (Co-Cr-Fe-Mg-Mn)$3O_4$ high entropy spinels. Journal of the European Ceramic Society, 2020. 40(4): p. 1644-1650.
44. Rost, C.M., et al., Entropy-stabilized transition metallic oxides. Nat. Commun., 2015. 6(2): p. 8495.
45. Yang, Y., et al., Investigation of thermodynamic properties of high entropy (Ta-Nb-Hf-Ti-Zr)C and (Ta-Nb-Hf-Ti-Zr)N. Journal of Alloys and Compounds, 2019. 788: p. 1076-1083.
46. Lužnik, J., et al., Complex magnetism of Ho-Dy-Y-Gd-Tb hexagonal high-entropy alloy. Physical Review B, 2015. 92(22): p. 224201.
47. Yang, X. and Y. Zhang, Prediction of high-entropy stabilized solid-solution in multi-component alloys. Journal of Materials Chemistry and Physics, 2012. 132(2-3): p. 233-238.
48. Mayrhofer, P.H., et al., High-entropy ceramic thin films; A case study on transition metal diborides. Scripta Materialia, 2018. 149: p. 93-97.
49. Yeh, J.-W., et al., Nanostructured High-Entropy Alloys with Multiple Principal Elements: Novel Alloy Design Concepts and Outcomes. Advanced Engineering Materials, 2004. 6: p. 299-303.
50. Lilova, K., et al., Thermodynamics of coal2oT coga2o4 solid solutions. Journal of Solid State Chemistry, 2010. 183: p. 1266-1271.
51. Sharma, A.S., et al., High-entropy alloys, and metallic nanocomposites: Processing challenges, microstructure development, and property enhancement. Materials Science and Engineering: R: Reports, 2018. 131: p. 1-42.
52. Vaidya, M., G.M. Muralikrishna, and B.S. Murty, High-entropy alloys by mechanical alloying: A review. Journal of Materials Research, 2019. 34(5): p. 664-686.
53. Yeh, J.-W., Recent progress in high-entropy alloys. Annales de Chimie Science des Matériaux, 2006. 31(6): p. 633-648.
54. Tsai, M.-H. and J.-W. Yeh, High-Entropy Alloys: A Critical Review. Materials Research Letters, 2014. 2(3): p. 107-123.
55. Singh, A.K. and A. Subramaniam, On the formation of disordered solid solutions in multi-component alloys. Alloys and Compounds, 2014. 587: p. 113-119.

56. Wang, F.J., Y. Zhang, and G.L. Chen, Atomic packing efficiency and phase transition in a high entropy alloy. Journal of Alloys and Compounds, 2009. 478(1-2): p. 321-324.
57. Cheng, B., et al., Pressure-induced tuning of lattice distortion in a high-entropy oxide. Communications Chemistry, 2019. 2(1): p. 1-9.
58. Yeh, J.-W., Alloy Design Strategies and Future Trends in High-Entropy Alloys. Jom, 2013. 65(12): p. 1759-1771.
59. Yeh, J.-W., Physical Metallurgy of High-Entropy Alloys. Jom, 2015. 67(10): p. 2254-2261.
60. Ng, C., et al., Entropy-driven phase stability and slow diffusion kinetics in an $Al_{0.5}CoCrCuFeNi$ high entropy alloy. Intermetallics, 2012. 31: p. 165-172.
61. Chen, H., et al., Mechanochemical Synthesis of High Entropy Oxide Materials under Ambient Conditions: Dispersion of Catalysts via Entropy Maximization. ACS Materials Letters, 2019. 1(1): p. 83-88.
62. Biesuz, M., et al., Synthesis and sintering of (Mg, Co, Ni, Cu, and Zn)O entropy-stabilized oxides obtained by wet chemical methods. Journal of Materials Science, 2018. 53(11): p. 8074-8085.
63. Chen, H., et al., Entropy-stabilized metal oxide solid solutions as CO oxidation catalysts with high-temperature stability. Journal of Materials Chemistry A, 2018. 6(24): p. 11129-11133.
64. Wuchina, E., et al., UHTCs: Ultra-High Temperature Ceramic materials for extreme environment applications. Journal of Electrochemical Society Interface, 2007. 16(4): p. 30-36.
65. Zhang, S., et al., Sintering Effect on Microstructure and Properties of (K, Na)NbO_3 Ceramics. Journal of the American Ceramic Society, 2011. 94(11): p. 3659-3665.
66. Wang, X.H., et al., Two-Step Sintering of Ceramics with Constant Grain-Size, II: $BaTiO_3$ and Ni-Cu-Zn Ferrite. Journal of the American Ceramic Society, 2006. 89(2): p. 438-443.
67. Hallmann, L., et al., Effect of dopants and sintering temperature on microstructure and low-temperature degradation of dental Y-TZP-zirconia. Journal of the European Ceramic Society, 2012. 32(16): p. 4091-4104.
68. Naceur, H., A. Megriche, and M. El Maaoui, Effect of sintering temperature on microstructure and electrical properties of $Sr_{1-x}(Na_{0.5}Bi_{0.5})_x$ $Bi_2Nb_2O_9$ solid solutions. Journal of Advanced Ceramics, 2014. 3(1): p. 17-30.

69. Rocha, E.P., et al., Mechanical behavior of ceramic veneer in zirconia-based restorations: a 3-dimensional finite element analysis using microcomputed tomography data. J Prosthet Dent, 2011. 105(1): p. 14-20.
70. Vikram, V., S. Nayar, and N. Reddy, Compressive Strength Evaluation between Metal ceramic and Zirconia crowns-An In-vitro Study. Indian Journal of Public Health Research & Development, 2019. 10(5): p. 284.
71. Quinn, G., Hardness testing of ceramics. Journal of Advanced Materials and Processes, 1998. 154: p. 23-27.
72. Bérardan, D., et al., Colossal dielectric constant in high entropy oxides. physical status solidi (RRL) - Rapid Research Letters, 2016. 10(4): p. 328-333.
73. Bérardan, D., et al., Room temperature lithium superionic conductivity in high entropy oxides. Journal of Materials Chemistry A, 2016. 4(24): p. 9536-9541.
74. Berardan, D., et al., Controlled Jahn-Teller distortion in (Mg-Co-Ni-Cu-Zn)O based high entropy oxides. Alloys and Compounds, 2017. 704: p. 693-700.
75. Mao, A., et al., Solution combustion synthesis and magnetic property of rock-salt $(Co_{0.2}Cu_{0.2}Mg_{0.2}Ni_{0.2}Zn_{0.2})O$ high-entropy oxide nanocrystalline powder. Journal of Magnetism and Magnetic Materials, 2019. 484: p. 245-252.
76. Djenadic, R., et al., Nebulized spray pyrolysis of Al-doped $Li_7La_3Zr_2O_{12}$ solid electrolyte for battery applications. Solid State Ionics, 2014. 263: p. 49-56.
77. Houshiar, M., et al., Synthesis of cobalt ferrite ($CoFe_2O_4$) nanoparticles using combustion, coprecipitation, and precipitation methods: A comparison study of the size, structural, and magnetic properties. Journal of Magnetism and Magnetic Materials, 2014. 371: p. 43-48.
78. Kumar, A., et al., Combustion synthesis of copper-nickel catalysts for hydrogen production from ethanol. Chemical Engineering Journal, 2015. 278: p. 46-54.
79. Nersisyan, H.H., et al., Combustion synthesis of zero, one, two and three-dimensional nanostructures: Current trends and future perspectives. Progress in Energy and Combustion Science, 2017. 63: p. 79-118.
80. Chen, H., et al., Coprecipitation synthesis and thermal conductivity of $La_2Zr_2O_7$. Journal of Alloys and Compounds, 2009. 480(2): p. 843-848.
81. Qiu, N., et al., A high entropy oxide $(Mg_{0.2}Co_{0.2}Ni_{0.2}Cu_{0.2}Zn_{0.2})O$ with superior lithium storage performance. Alloys and Compounds, 2019. 777: p. 767-774.

82. Sarkar, A., et al., Multicomponent equiatomic rare earth oxides with a narrow bandgap and associated praseodymium multivalency. Journal of Dalton Trans, 2017. 46(36): p. 12167-12176.
83. Jiang, S., et al., A new class of high-entropy perovskite oxides. Scripta Materialia, 2018. 142: p. 116-120.
84. Spiridigliozzi, L., et al., Effect of the Precipitating Agent on the Synthesis and Sintering Behavior of 20 mol% Sm-Doped Ceria. Advances in Materials Science and Engineering, 2016. 2016: p. 1-8.
85. Chu, L., et al., High-performance NiO microsphere anode assembled from porous nanosheets for lithium-ion batteries. RSC Advances, 2015. 5(61): p. 49765-49770.
86. Aziz, B.K. and M.A.H. Karim, Efficient catalytic photodegradation of methylene blue from medical lab wastewater using MgO nanoparticles synthesized by direct precipitation method. Journal of Reaction Kinetics, Mechanisms and Catalysis, 2019. 128(2): p. 1127-1139.
87. Zaidi, B., et al., Investigation on Synthesis of MgO Powder by Liquid Phase method. Metallofizika i noveĭshie tekhnologii, 2019. 41: p. 1121–1126.
88. Ravi Dhas, C., et al., Visible light-driven photocatalytic degradation of Rhodamine B and Direct Red using cobalt oxide nanoparticles. Ceramics International, 2015. 41(8): p. 9301-9313.
89. Sharifi, S., et al., Characterization of Cobalt Oxide Co_3O_4 Nanoparticles Prepared by Various Methods: Effect of Calcination Temperatures on Size, Dimension and Catalytic Decomposition of Hydrogen Peroxide, 2013. 9(1): p. 51-58.
90. Manouchehri, I., P. Kameli, and H. Salamati, Facile Synthesis of Co_3O_4/CoO Nanoparticles by Thermal Treatment of Ball-Milled Precursors. Journal of Superconductivity and Novel Magnetism, 2011. 24(6): p. 1907-1910.
91. Maria Fernanda Gazulla, et al., Characterization of Cobalt-Oxides Transformations with Temperature at Different Atmospheres. International Journal of Chem Sci, 2019. 17(3): p. 312.
92. Ahamed, A.J., P.V. Kumar, and M. Karthikeyan, Wet chemical synthesis and characterization of NiO nanoparticles. Int. Journal of Nano. Corr. Sci. Engg, 2015. 2(5): p. 31-38.

93. Kumar, P., A. Jafar Ahamed, and M. Karthikeyan, Synthesis and characterization of NiO nanoparticles by chemical as well as green routes and their comparisons concerning the cytotoxic effect and toxicity studies in microbial and MCF-7 cancer cell models. SN Applied Sciences, 2019. 1(9): p. 1-15.
94. Phiwdang, K., et al., Synthesis of CuO Nanoparticles by Precipitation Method Using Different Precursors. Energy Procedia, 2013. 34: p. 740-745.
95. Manyasree, D., Kiran Mayi Peddi, and R. Ravikumar. CuO nanoparticles: synthesis, characterization, and their bactericidal efficacy. International Journal of Applied Pharmaceutics, 2017. 9(6): p. 71-74.
96. Wasly, H.S., M.S.A. El-Sadek, and K.M. Batoo, Novel synthesis, structural, optical properties and antibacterial activity of ZnO nanoparticles. Materials Research Express, 2019. 6(5): p. 055003.
97. Parra, M.R. and F.Z. Haque, Aqueous chemical route synthesis and the effect of calcination temperature on the structural and optical properties of ZnO nanoparticles. Journal of Materials Research and Technology, 2014. 3(4): p. 363-369.
98. Rost, C., et al., Local structure of the $(Mg_xNi_xCo_xCu_xZn_x)O$ (x=0.2) entropy-stabilized oxide: An EXAFS study. Journal of the American Ceramic Society, 2017. 100: p. 2732-2738.
99. Dupuy, A.D., X. Wang, and J.M. Schoenung, Entropic phase transformation in nanocrystalline high entropy oxides. Journal of Materials Research Letters, 2018. 7(2): p. 60-67.
100. Hong, W., et al., Microstructural evolution and mechanical properties of (Mg-Co-Ni-Cu-Zn)O high-entropy ceramics. Journal of the American Ceramic Society, 2018. 102(4): p. 2228-2237.
101. Coelho, A., TOPAS, and TOPAS-Academic: an optimization program integrating computer algebra and crystallographic objects written in C++. Journal of Applied Crystallography, 2018. 51(1): p. 210-218.
102. Mofokeng, S.J., et al., Thermoluminescence properties of MgO: Al^{3+}, Li^{+} prepared by microwave-assisted solution combustion method. Physica B: Condensed Matter, 2020. 582: p. 412008.
103. Mirzaei, H., et al., Direct growth of ternary copper nickel cobalt oxide nanowires as a binder-free electrode on carbon cloth for nonenzymatic glucose sensing. Microchemical Journal, 2018. 142: p. 343-351.

104. Nguyen, K., et al., A comparative study on the electrochemical properties of nanoporous nickel oxide nanowires and nanosheets prepared by a hydrothermal method. RSC Advances, 2018. 8: p. 19449-19455.
105. Sathyanathan, S., K. Sivakumaran, and K. Jayamoorthy, FTIR and multivariate analysis to study the effect of bulk and nano copper oxide on peanut plant leaves. Journal of Science: Advanced Materials and Devices, 2016. 1(3): p. 343-350.
106. Arefi, M. and S. Rezaei-Zarchi, Synthesis of Zinc Oxide Nanoparticles and Their Effect on the Compressive Strength and Setting Time of Self-Compacted Concrete Paste as Cementitious Composites. International journal of molecular sciences, 2012. 13: p. 4340-50.
107. Davies, P.K. and A. Navrotsky, Thermodynamics of solid solution formation in NiO□MgO and NiO□ZnO. Solid State Chemistry, 1981. 38(2): p. 264-276.
108. Bergmann, C. and A. Stumpf, Microstructure of Ceramic Materials. In Dental Ceramics, 2013. p. 31-44.
109. Khadivi Ayask, H., J. Vahdati Khaki, and M. Haddad Sabzevar, Facile Synthesis of Copper Oxide Nanoparticles using Copper hydroxide by the mechanochemical process. journal of ultrafine-grained and nanostructured materials, 2015. 48(1): p. 37-44.
110. El-Shobaky, G.A., et al., Thermal decomposition of basic cobalt and copper carbonates. Journal of thermal analysis, 1996. 46(6): p. 1801-1808.
111. Brown, I.W.M., K.J.D. Mackenzie, and G.J. Gainsford, Thermal decomposition of the basic copper carbonates malachite and azurite. Thermochimica Acta, 1984. 75(1): p. 23-32.
112. Klein, A. and D. Hotza, Advanced ceramics with dense and fine-grained microstructures through fast firing. Reviews on Advanced Materials Science, 2012. 30(273): p. e281.
113. Pratten, N.A., The precise measurement of the density of small samples. Journal of Materials Science, 1981. 16(7): p. 1737-1747.
114. Raheem, Z., Standard Test Methods for Apparent Porosity, Water Absorption, Apparent Specific Gravity, and Bulk Density of Burned Refractory Brick and Shapes by Boiling Water 1. 2019.
115. Gild, J., et al., High-entropy fluorite oxides. Journal of the European Ceramic Society, 2018. 38(10): p. 3578-3584.

APPENDIX

In this part, we have tried to generalize the data which were not mentioned in the main body of this thesis works.

Appendix A: XRD Patterns of Individual Binary Oxides.

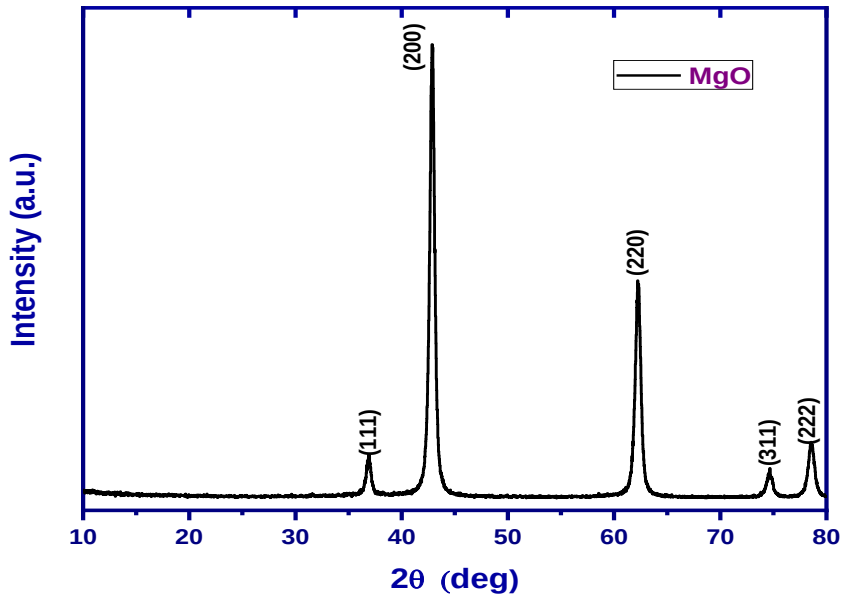

Figure A.1: *XRD patterns of Magnesium Oxide.*

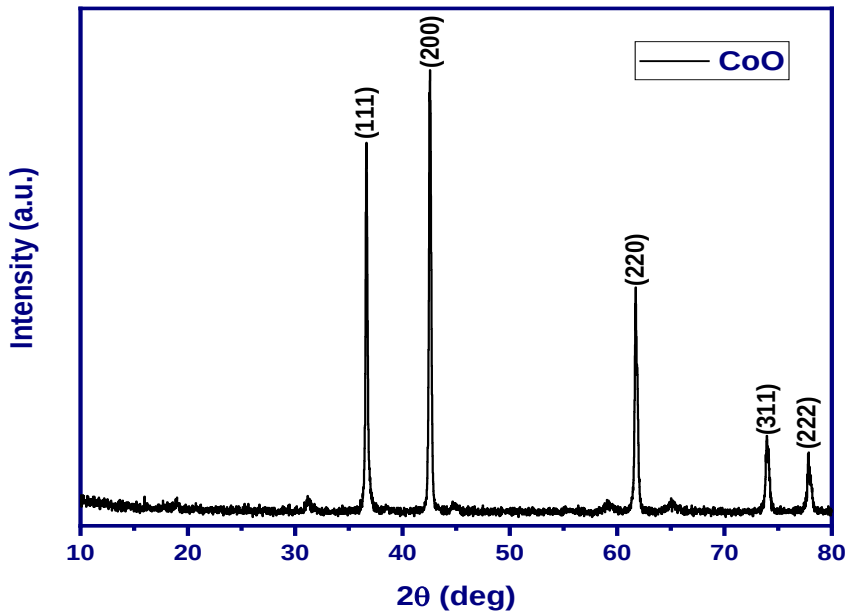

Figure A.2: *XRD patterns of Cobalt Oxide.*

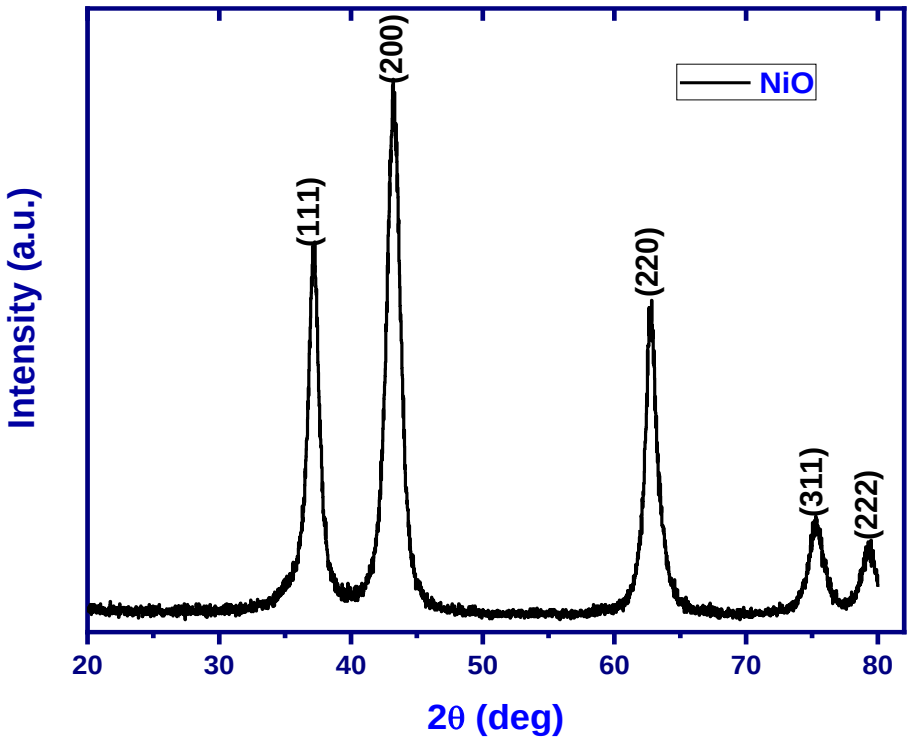

Figure A.3: *XRD patterns of Nickel Oxide.*

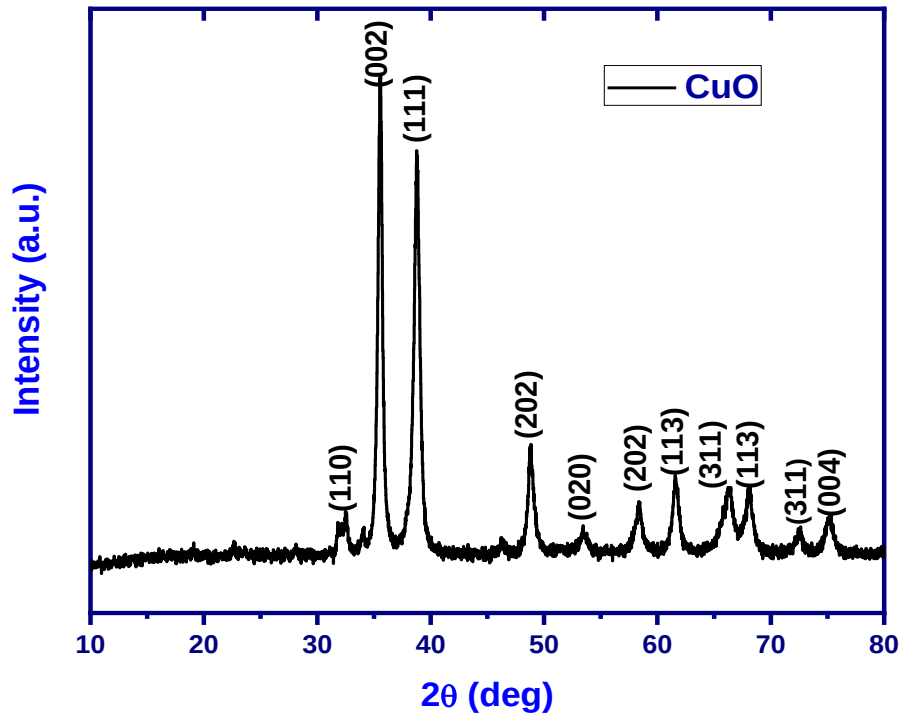

Figure A.4: *XRD patterns of Copper Oxide.*

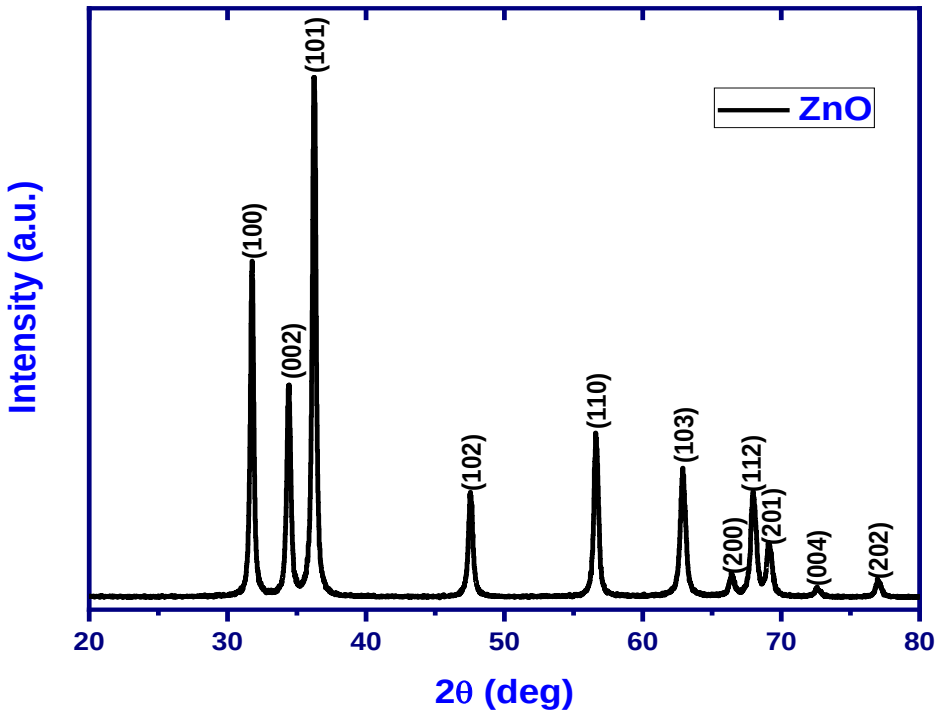

Figure A.5: *XRD patterns of Zinc Oxide.*

Appendix B: Optical Images of Vickers Indentations.

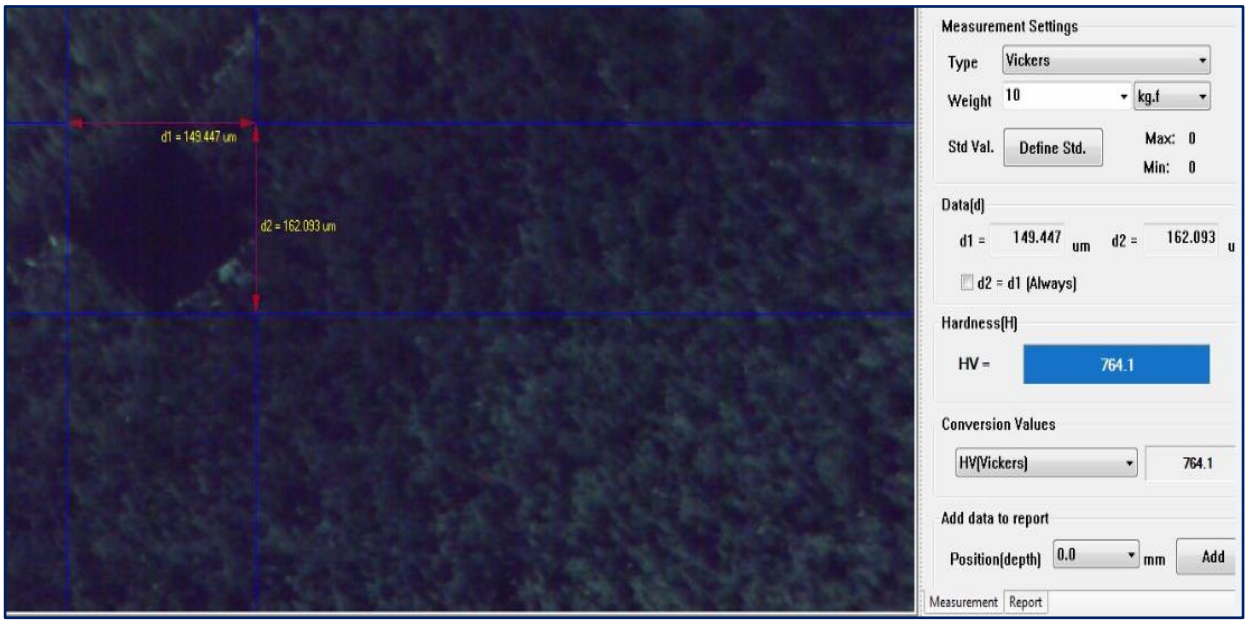

Figure B.1: *Optical images of HEO pellet sintered at 1100 ℃ for 9 h.*

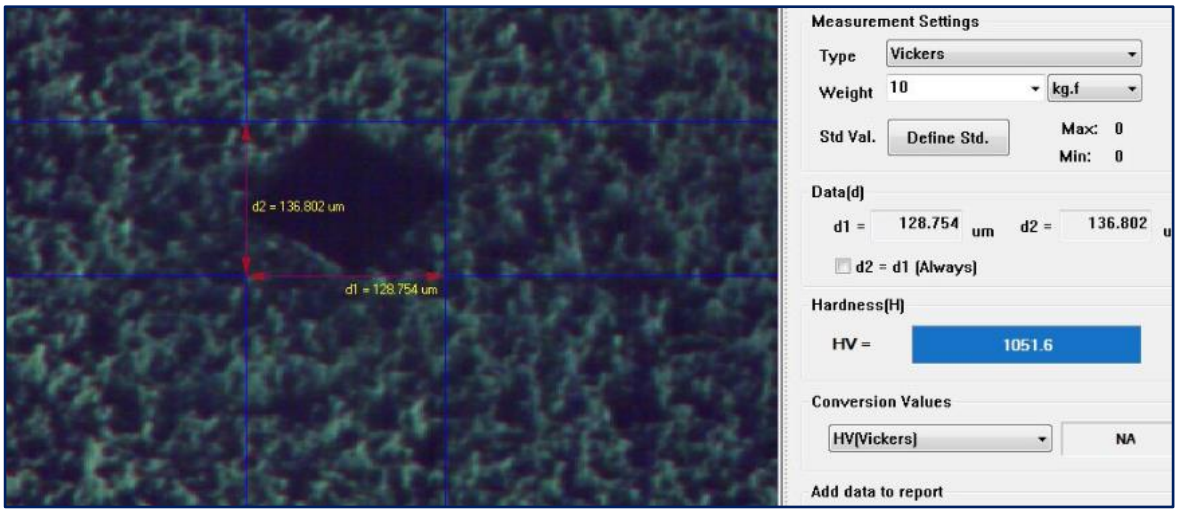

Figure B.2: *Optical images of HEO pellet sintered at 1100 ℃ for 15 h.*

Figure B.3: *Optical images of HEO pellet sintered at 1200 ℃ for 9 h.*

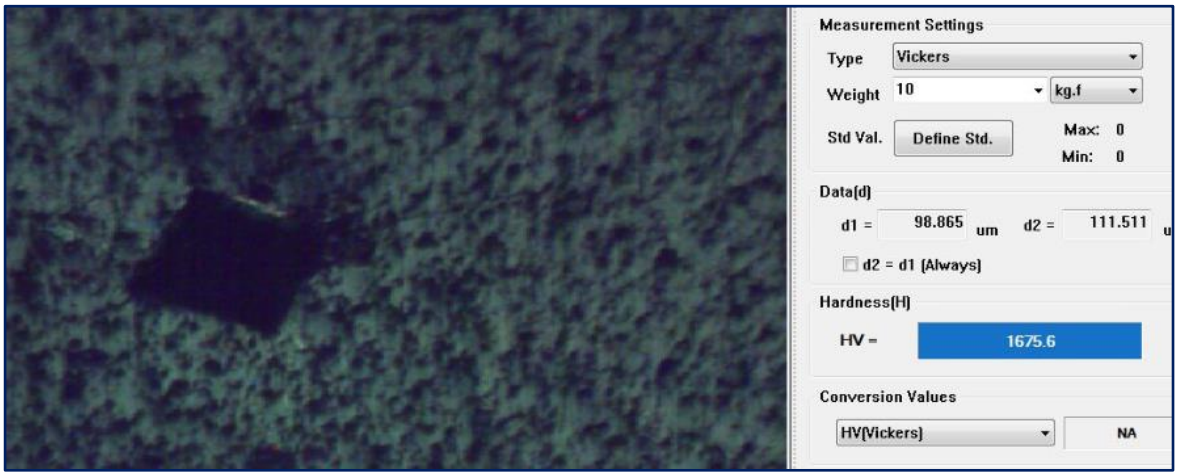

Figure B.4: *Optical images of HEO pellet sintered at 1200 ℃ for 15 h.*

Appendix C: Raw Data for Thermal Analysis Results.

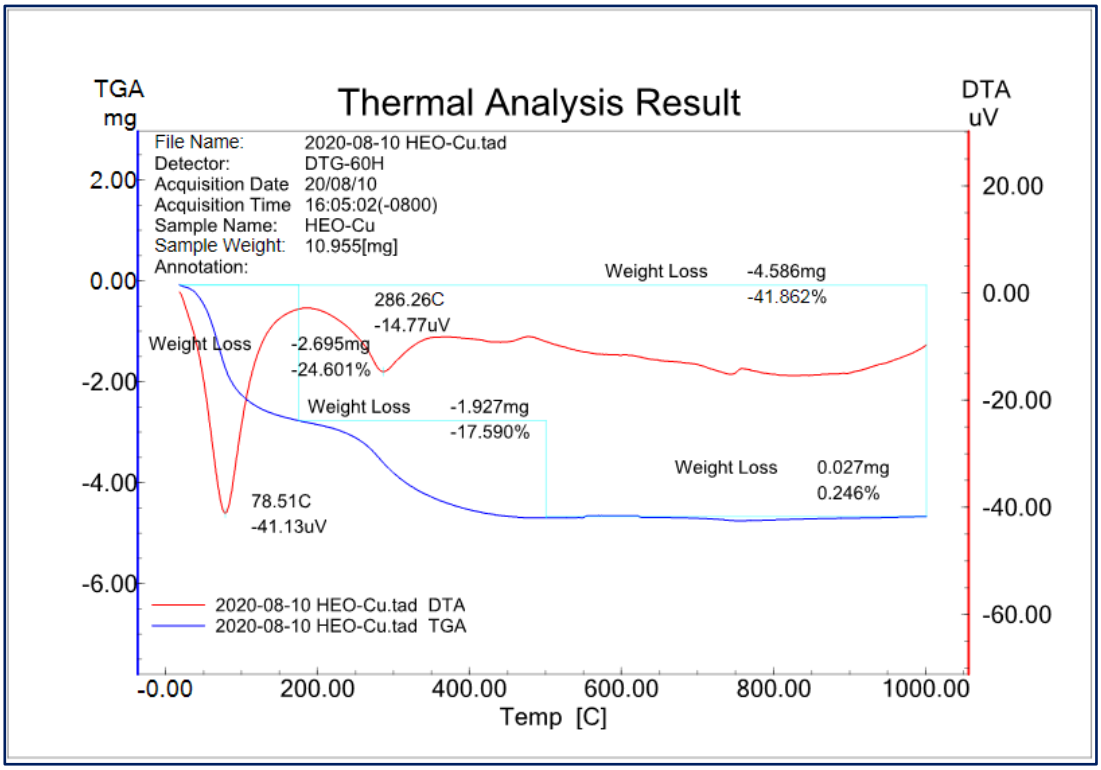

Figure C.1: *Thermal Analysis of pre-alloyed HEO powders (as ball milled).*

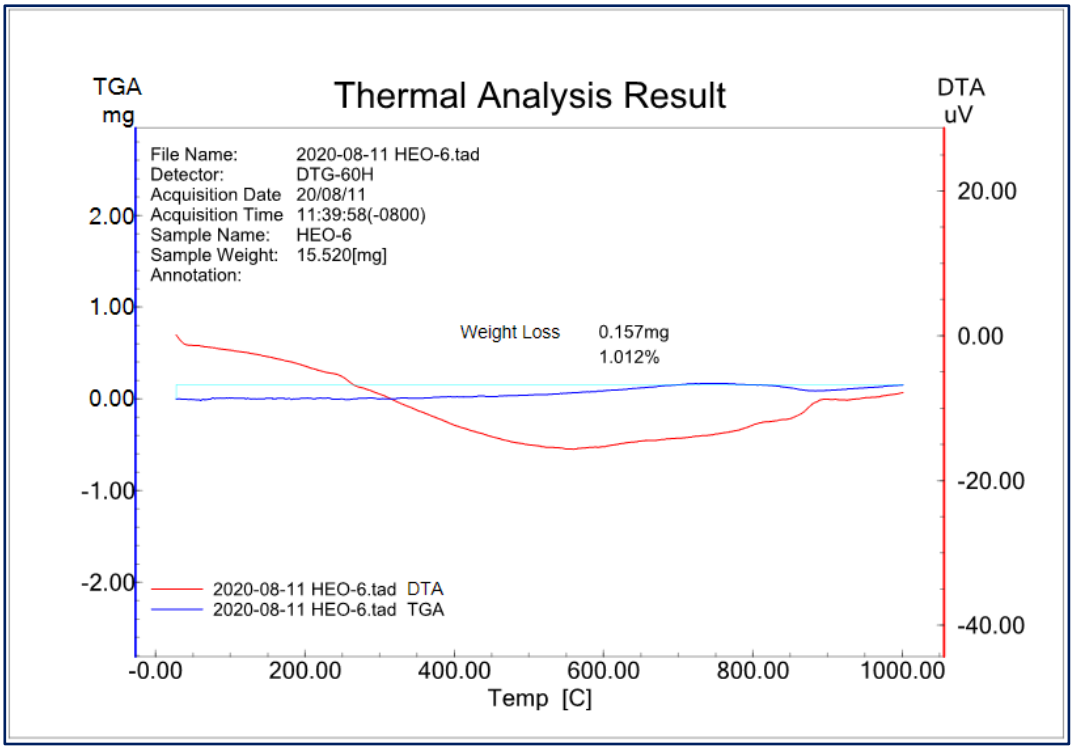

Figure C.2: *Thermal Analysis of as-synthesized HEO powders (calcined at 950 ℃).*

Appendix D: Engineering Stress-Strain Diagrams for Compression Test of HEO.

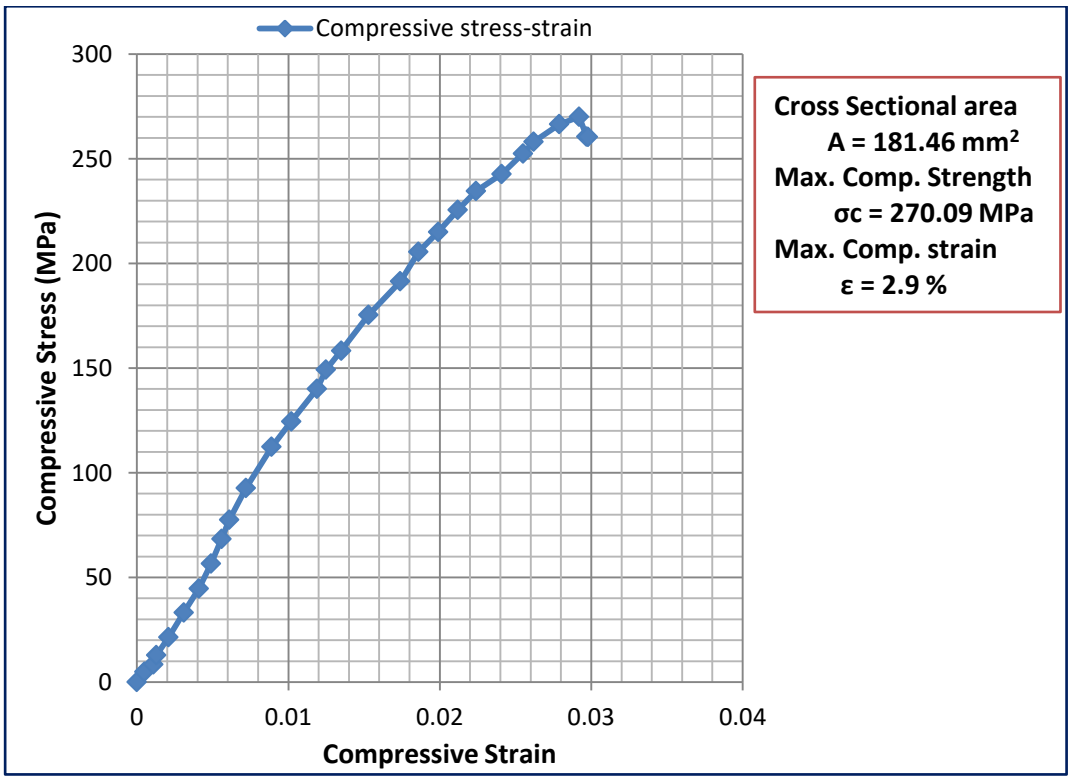

Figure D.1: *Compression stress-strain curve for HEO sample sintered at 1200 ℃ for 15h.*

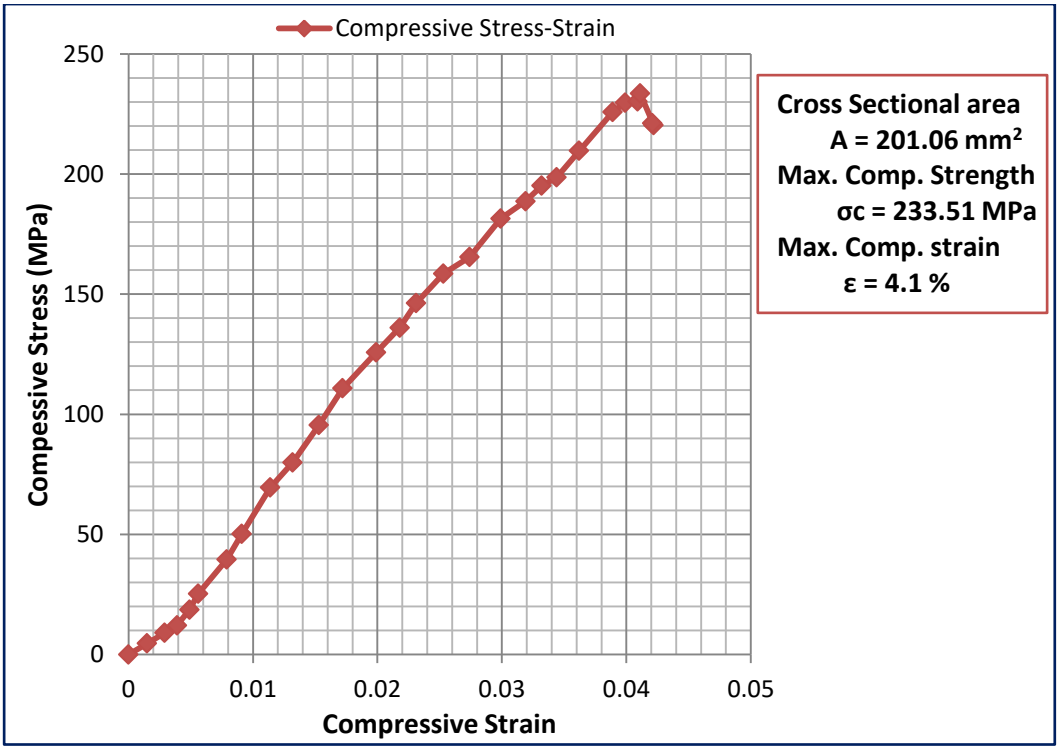

Figure D.2: *Compression stress-strain curve for HEO sample sintered at 1100 ℃ for 15h.*